JACS
JOURNAL OF THE AMERICAN CHEMICAL SOCIETY
pubs.acs.org/JACS

Article

Dynamic *In Vivo* Mapping of the Methylproteome Using a Chemoenzymatic Approach

Jonathan Farhi,◆ Benjamin Emenike,◆ Richard S. Lee, Kirti Sad, Dorelle V. Fawwal, Christian M. Beusch, Robert B. Jones, Ashish K. Verma, Celina Y. Jones, Maryam Foroozani, Monica Reeves, Kiran K. Parwani, Pritha Bagchi, Roger B. Deal, David J. Katz, Anita H. Corbett, David E. Gordon, Monika Raj, and Jennifer M. Spangle*

Cite This: *J. Am. Chem. Soc.* 2025, 147, 7214–7230

Read Online

ACCESS | Metrics & More | Article Recommendations | Supporting Information

ABSTRACT: Dynamic protein post-translational methylation is essential for cellular function, highlighted by the essential role of methylation in transcriptional regulation and its aberrant dysregulation in diseases, including cancer. This underscores the importance of cataloging the cellular methylproteome. However, comprehensive analysis of the methylproteome remains elusive due to limitations in current enrichment and analysis pipelines. Here, we employ an L-methionine analogue, ProSeMet, that is chemoenzymatically converted to the SAM analogue ProSeAM in cells and *in vivo* to tag proteins with a biorthogonal alkyne that can be directly detected via liquid chromatography and tandem mass spectrometry (LC-MS/MS), or functionalized for subsequent selective enrichment and LC-MS/MS identification. Without enrichment, we identify known and novel lysine mono-, di-, and tripargylation, histidine propargylation, and arginine propargylation with site-specific resolution on proteins including heat shock protein HSPA8, the translational elongation factor eEF1A1, and the metabolic enzyme phosphoglycerate mutase 1, or PGAM1, for which methylation has been implicated in human disease. With enrichment, we identify 486 proteins known to be methylated and 221 proteins with novel propargylation sites encompassing diverse cellular functions. Systemic ProSeMet delivery in mice propargylates proteins across organ systems with blood–brain barrier penetrance and identifies site-specific propargylation *in vivo* with LC-MS/MS. Leveraging these pipelines to define the cellular methylproteome may have broad applications for understanding the methylproteome in the context of disease.

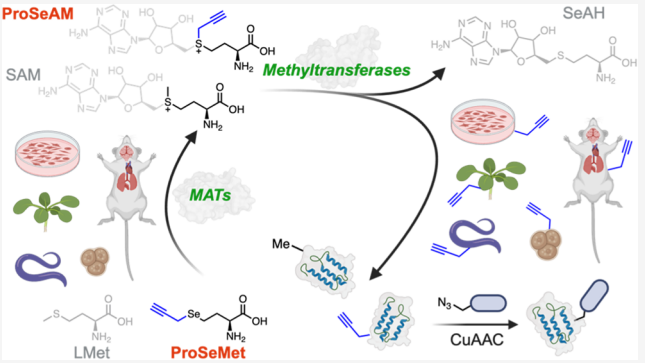

INTRODUCTION

Protein methylation is a widely occurring post-translational modification (PTM) that plays an important role in cell signaling, development, and disease.[1] Methylation most commonly occurs on the basic amino acids lysine (Lys), arginine (Arg), and histidine (His): lysine residues can be mono-, di-, or trimethylated, arginine residues can be monomethylated or dimethylated symmetrically or asymmetrically, and histidine is monomethylated at both the 1 and 3 positions of the imidazole ring.[1,2] On proteins, these methylation events are catalyzed by methyltransferase enzymes using the metabolite *S*-adenosyl-L-methionine (SAM).[3] SAM-dependent methyltransferases fall into three structurally distinct classes: Class I enzymes contain a conserved seven-stranded β-sheet and include all canonical arginine methyltransferases (PRMTs) as well as the lysine methyltransferase DOT1L; Class II enzymes contain a SET domain and encompass all other lysine methyltransferases (KMTs), and Class III enzymes are membrane-associated methyltransferases.[4]

Histone protein methylation affects epigenetic regulation of gene expression by mediating the recruitment of chromatin-modifying enzymes to chromatin and transcriptional regulators to gene regulatory regions including promoters and enhancers.[2,5] Nonhistone protein methylation is likewise an essential PTM affecting cellular biology and disease pathogenesis.[6,7] For example, methylation of the PI3K effector AKT by SETDB1 increases the duration of AKT activation, promoting tumor growth in murine models.[8] Similarly, methylation of CRAF at R100 by PRMT6 interferes with RAS/RAF binding, suggesting a mechanism by which PRMT6 loss increases tumor initiation and metastasis in hepatocellular

Received: June 17, 2024
Revised: February 11, 2025
Accepted: February 12, 2025
Published: February 25, 2025

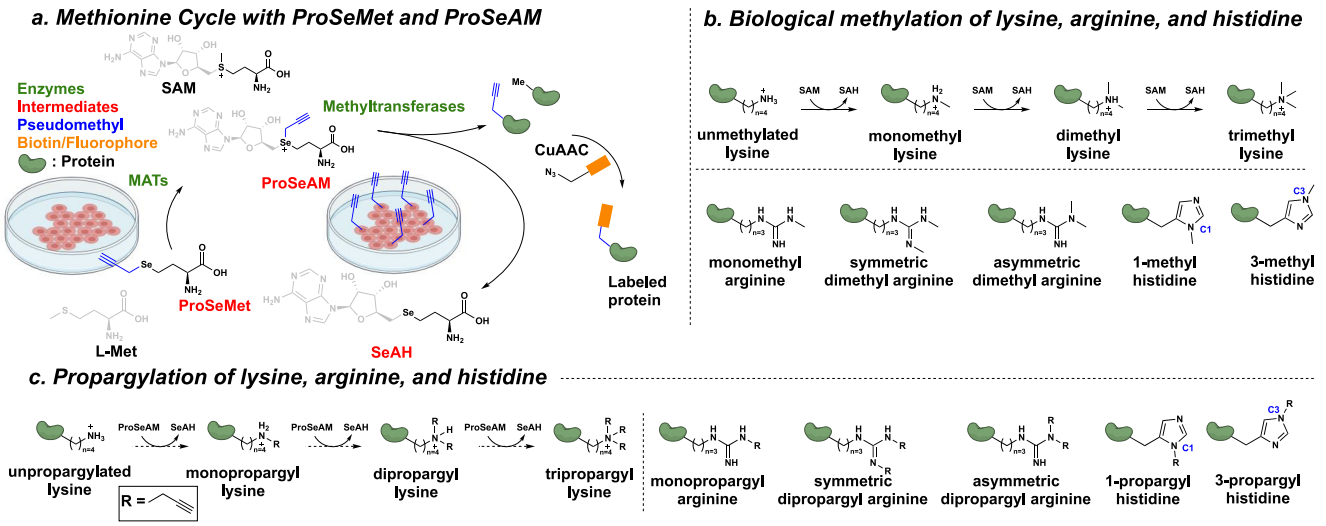

Figure 1. Chemoenzymatic approach for metabolic Methyltransferase labeling. **a**. ProSeMet can be converted to ProSeAM by MAT enzymes in live cells. ProSeAM can then be used by diverse methyltransferases to propargylate target protein. **b**. (top panel) Conversion of unmethylated lysine to mono, di, and trimethyl-Lys through the action of SAM. (bottom panel) The guanidine moiety on Arg can undergo monomethylation, then symmetric or asymmetric dimethylation. The imidazole ring of His can undergo monomethylation at the C1 or C3 position **c**. (left panel) Conversion of unpropargylated Lys to mono, di, and tripropargyl lysine could occur through the intermediacy of ProSeAM. (right panel) Predicted Arg monopropargylation, symmetric dipropargylation, and asymmetric dipropargylation as well as His propargylation at the C1 and C3 positions.

carcinoma.[9] Moreover, the oncogenic role of enhancer of zester homologue 2 (EZH2) is hypothesized to extend beyond methylation of histone H3 on lysine 27 (H3K37) to include cytosolic targets: the transcription factors STAT3,[10] GATA4 (K299);[11] and FOXA1 (K295),[12] among others. The important roles these methyltransferase enzymes play in normal cellular function and disease has prompted the clinical development of several inhibitors, including the recent first-in-class EZH2 inhibitor tazemetostat for the treatment of epithelioid sarcoma and follicular lymphoma[13] and several PRMT1/5 and CARM1 inhibitors.[14]

Current efforts to identify histone and nonhistone protein methylation often employ mass spectrometry (MS) or antibody-based approaches to identify methylated residues and changes to their methylation status.[6] However, unlike acetylation or phosphorylation, methylation does not change the charge or physiochemical properties of the amino acid residue, rendering MS-based characterization challenging without isotopic labeling, chemical modification, or biased enrichment to reduce the complexity of analysis.[1,15] The development of pan-methyl, pan-methyl-lysine, and pan-methyl-arginine specific antibodies has underscored the breadth of the methylproteome[16,17] but has been limited by cross-reactivity (e.g., between methylated Lys and Arg residues),[18] batch-to-batch irreproducibility, and an inability to identify novel methylation sites.[19] Furthermore, MS-based methods aimed at detecting methylation must overcome high false discovery rates because a high number of amino acid combinations produce sequences that are isobaric to methylated peptides of a different sequence (e.g., the mass difference between Asp and Glu is equivalent to a single methylation event).[20]

The challenges presented by current MS- or antibody-based approaches have prompted the development of chemical strategies to selectively modify methylated residues[21] or hijack cellular machinery for a tag-and-modify approach.[22] In particular, SAM analogues have been employed to "pseudo-methylate" (tag) proteins using engineered methyltransferases in live cells or on cell lysate.[23−25] Recently, treatment of cell lysates with the SAM analogue propargyl-*Se*−adenosyl-L-selenomethionine (ProSeAM) enabled profiling of the methylproteome and of methylhistidine targets of the histidine methyltransferase METTL9.[26,27] While these *in situ* methodologies demonstrate the ability of selected methyltransferases to methylate a substrate based on a consensus sequence, *in situ* studies cannot capture changes to the methylproteome in response to biological stimuli or reflect methyltransferase activation and localization into unique cellular compartments. Likewise, strategies involving engineered enzymes are unable to profile the broad spectrum of the methylproteome and are therefore restricted to specific applications.

These challenges have prompted the development of novel strategies to chemically label methyltransferase targets in live cells. The L-Met analogue propargyl-L-selenohomocysteine (ProSeMet) is chemoenzymatically converted by cellular methionine adenosyltransferase (MAT) enzymes to the SAM analogue ProSeAM *in vitro*. In turn, ProSeAM is used by native RNA methyltransferases to propargylate RNA with a biorthogonal alkyne tag allowing for downstream analysis.[28−30] Previous reports have not explored, however, the ability of ProSeAM to propargylate proteins using endogenous methyltransferases. As such, we envisioned that dynamic profiling of the methylproteome could be accomplished using ProSeMet through a chemoenzymatic approach (Figure 1). In this work, we describe the application of ProSeMet for methylproteome profiling *in vitro* and *in vivo*. Using ProSeMet, we performed an unbiased analysis of the propargylproteome as a surrogate for the methylproteome with and without enrichment in the SMARCB1 mutant, EZH2-activated, cell line G401.[31] Prior to enrichment, we identified arginine, lysine, and histidine propargylation with site-specific resolution including heat shock protein HSPA8 at R469. Following functionalization and enrichment, we identified 486 previously characterized methylated proteins and discovered 221 novel propargylated proteins. Furthermore, we demonstrate that *in vivo* ProSeMet administration to a variety of living organisms including

https://doi.org/10.1021/jacs.4c08175
J. Am. Chem. Soc. 2025, 147, 7214−7230

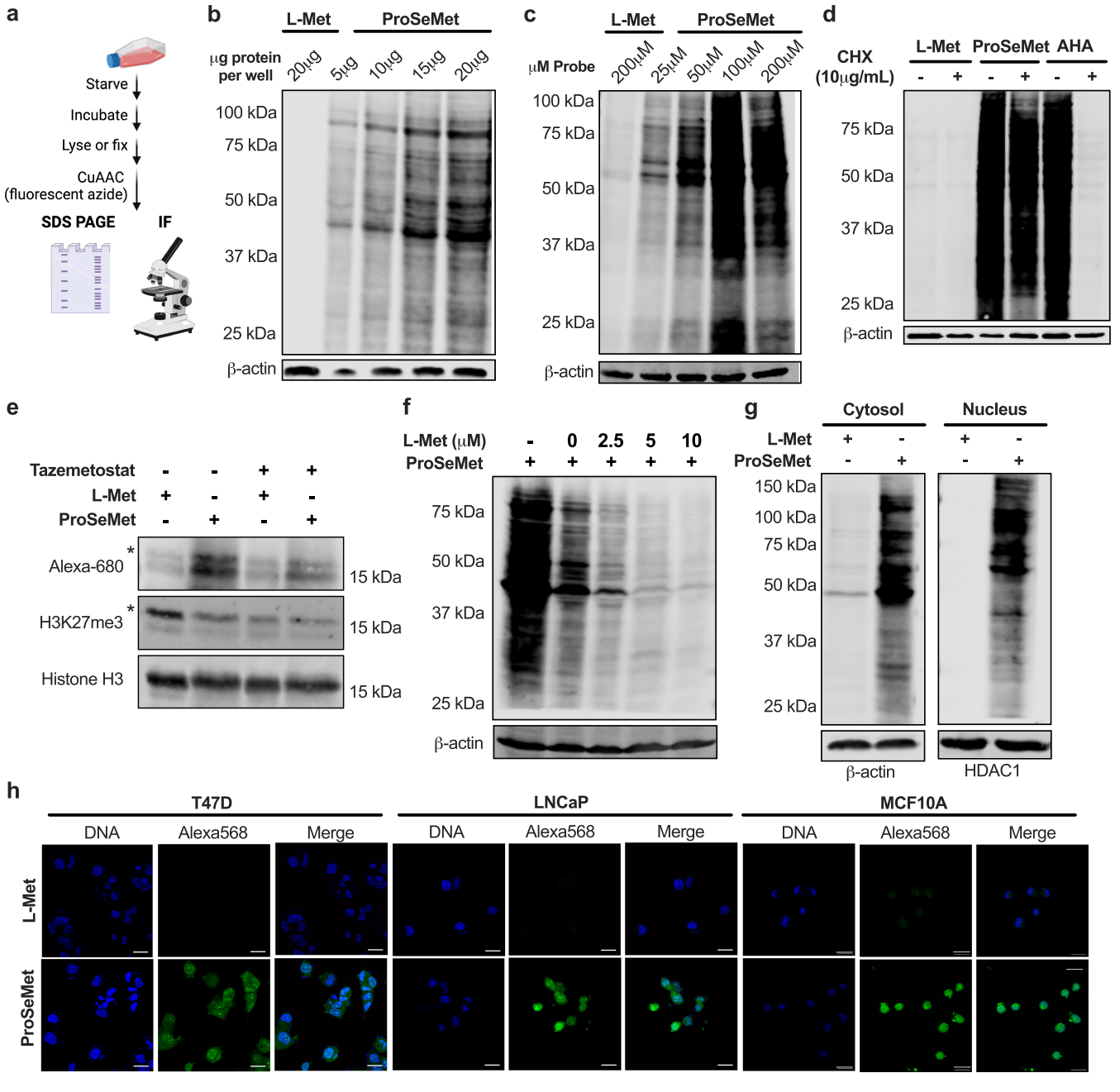

Figure 2. ProSeMet propargylates nuclear and cytosolic proteins in live cells. **a.** Workflow for gel- and IF-based profiling of ProSeMet target proteins. Cells were starved of L-Met by incubating for 30 min in L-Met-free media. Cells were then lysed or fixed, subjected to CuAAC to attach a fluorophore, and separated via SDS-PAGE or imaged via confocal microscopy. **b.** T47D cells treated with 100 μM ProSeMet or 100 μM L-Met for 16 h were lysed and subjected to the click reaction to attach a fluorescent picolyl azide (680 nm). Increasing protein concentration (5−20 μg) was loaded into each well and separated by SDS-PAGE. (n = 3). **c.** T47D cells were treated with 200 μM L-Met or increasing concentration (25−200 μM) ProSeMet 16 h. Cellular lysates were subjected to CuAAC and separated via SDS-PAGE. (n = 3). **d.** T47D cells were treated with 100 μM L-Met, ProSeMet, or AHA in the presence or absence of 10 μg/mL of cycloheximide (CHX). After 16 h, lysates were collected and subjected to CuAAC to attach a fluorescent picolyl azide (L-Met, ProSeMet) or fluorescent alkyne (AHA) then separated by SDS-PAGE (n = 3). **e.** G401 cells were starved of L-Met by incubating for 30 min in L-Met Free media. Cells were then treated with 1 μM tazemetostat or DMSO for 72 h, after which histones were acid extracted and used for CuAAC to attach a fluorescent picolyl azide (680 nm). Resulting lysates were separated via SDS-PAGE and directly imaged or immunoblotted with the indicated antibodies. *, indicated protein, (n = 2). **f.** Competition by increasing concentrations of L-Met during 16 h incubation of T47D cells with 100 μM ProSeMet reduces ProSeMet labeling across molecular weights and in a dose-dependent manner (n = 3). **g.** Cell fractionation of T47D cells treated with 100 μM ProSeMet or 100 μM L-Met for 16 h. (n = 3). **h.** T47D, LNCaP, and MCF10A cells were treated with 100 μM ProSeMet or 100 μM L-Met 16 h then fixed, permeabilized, subjected to CuAAC to attach a fluorescent picolyl azide (568 nm, pseudocolored green), and counterstained with Hoechst (blue). (n = 3).

Arabidopsis thaliana, *Caenorhabditis elegans*, *Saccharomyces cerevisiae*, and *Mus musculus* resulted in protein propargylation. Specifically, ProSeMet administration to BALB c/J mice leads to labeling and identification of site-specific propargylation via liquid chromatography and tandem mass spectrometry (LC-MS/MS) in all organ systems analyzed, including the heart,

https://doi.org/10.1021/jacs.4c08175
J. Am. Chem. Soc. 2025, 147, 7214−7230

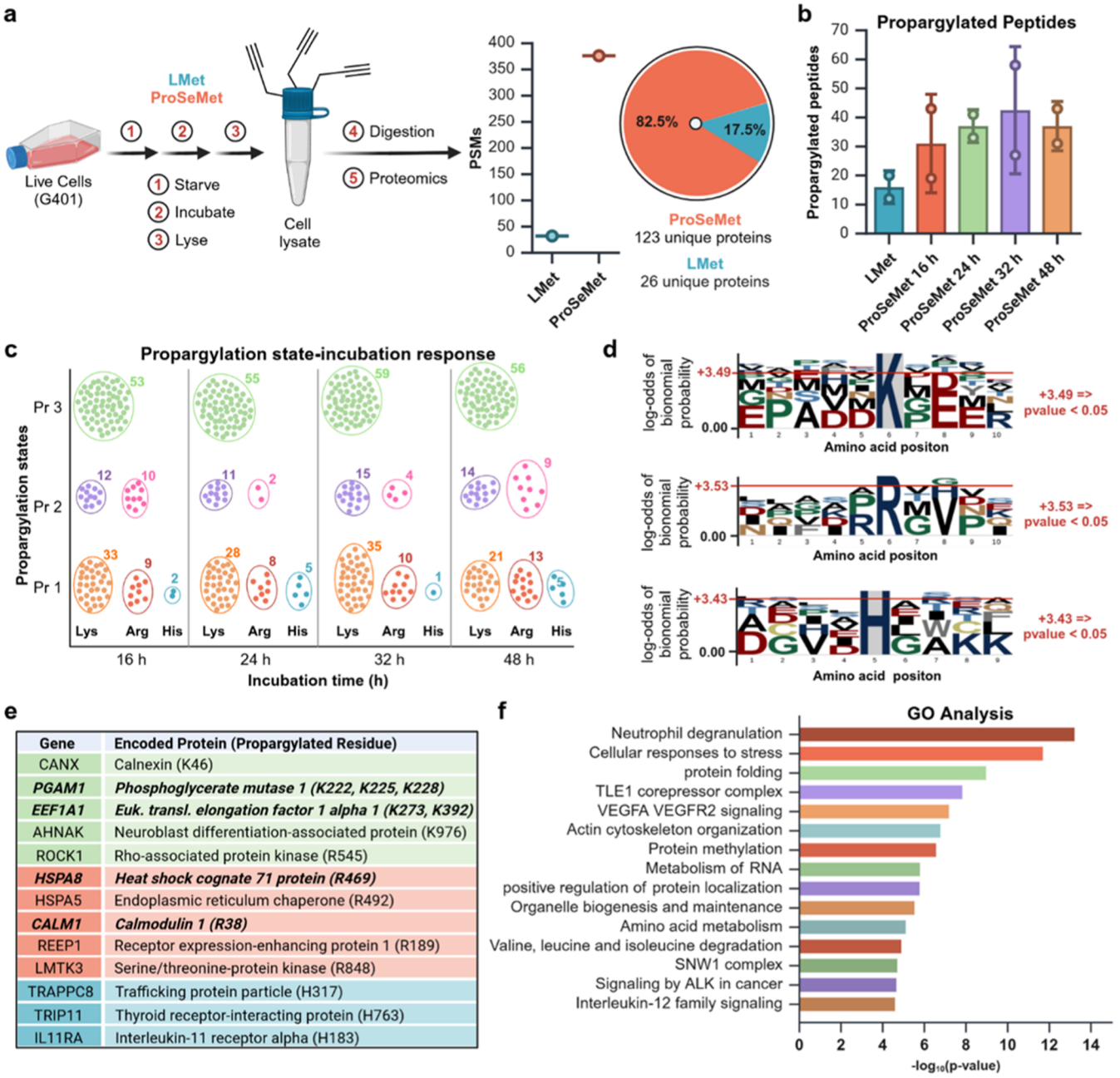

Gene	Encoded Protein (Propargylated Residue)
CANX	Calnexin (K46)
PGAM1	***Phosphoglycerate mutase 1 (K222, K225, K228)***
EEF1A1	***Euk. transl. elongation factor 1 alpha 1 (K273, K392)***
AHNAK	Neuroblast differentiation-associated protein (K976)
ROCK1	Rho-associated protein kinase (R545)
HSPA8	***Heat shock cognate 71 protein (R469)***
HSPA5	Endoplasmic reticulum chaperone (R492)
CALM1	***Calmodulin 1 (R38)***
REEP1	Receptor expression-enhancing protein 1 (R189)
LMTK3	Serine/threonine-protein kinase (R848)
TRAPPC8	Trafficking protein particle (H317)
TRIP11	Thyroid receptor-interacting protein (H763)
IL11RA	Interleukin-11 receptor alpha (H183)

Figure 3. Protein propargylation is mapped with site-specific resolution. All experiments and analyses were performed with two biological replicates ($n = 2$). **a**. Approach schematic. G401 cells treated with 100 μM ProSeMet with 100 μM L-Met for 16, 24, 36, or 48 h were lysed and processed for LC-MS/MS. MS raw files were searched against the human Swiss-Prot database (20,456 entries), with variable mass shifts of (+38.0157 Da for monopropargyl, +76.0314 Da for dipropargyl, and +114.0471 Da for tripropargyl) on lysine, arginine, and histidine, with a maximum propargylation state of 3 on lysine, 2 on arginine, and 1 on histidine. Proteomics analysis identified a total of 376 peptide spectral matches (PSMs) corresponding to 149 total proteins. Of these, 123 (82.5%) unique propargylated proteins were defined in ProSeMet-treated samples and 27 PSMs (26 proteins, 17.5%) for L-Met. **b**. Total number of propargylated peptides identified via LC-MS/MS across all time points, compared to L-Met. Data are represented as mean+SD **c**. Density plot of peptide propargylation states over the indicated time course. **d**. Sequence motif analysis of propargylated lysine, arginine, and histidine residues. Sequences containing 5 residues from the left and 4 residues from the right of modified lysine and arginine sites were utilized, with lysine or arginine as the fixed positions where $p < 0.05$. For sequence motif analysis of histidine, sequences containing 4 residues from the left and 4 residues from the right of modified histidine sites were utilized. The sequence motif was generated using the "probability logo generator for biological sequence motif" pLogo v1.2.0 **e**. Representative proteins propargylated in response to ProSeMet incubation and corresponding mapped sites of propargylation. Green, lysine propargylation events; red, arginine propargylation events; blue, histidine propargylation events. **f**. Gene ontology (GO) and pathway-process enrichment analysis of propargylated proteins in response to ProSeMet treatment. Gene list of propargylated proteins were utilized as input in metascape, with input and analysis species set to *Homo sapiens*. Pathway and process enrichment analysis was carried out with the following ontology sources: KEGG pathway, GO biological processes, Reactome Gene Sets, Canonical pathways, CORUM, WikiPathways, and PANTHER pathway. All genes in the human genome were used as the enrichment background. Terms with $p < 0.01$, a minimum count of 3, and an enrichment factor >1.5 were utilized. p-values were calculated based on the cumulative hypergeometric distribution, and q-values are calculated using the Benjamini–Hochberg procedure.

https://doi.org/10.1021/jacs.4c08175
J. Am. Chem. Soc. 2025, 147, 7214–7230

lungs, and brain. Our work demonstrates the development of an improved chemoenzymatic platform that has the potential to study dynamic changes to the methylproteome in response to biological stimulus and disease pathogenesis in both cell and murine models.

RESULTS

ProSeMet Competes with L-Met to Propargylate Proteins in the Cytoplasm and Nucleus. Previous literature has reported the use of ProSeMet as a viable substrate of the unaltered RNA methyltransferase METTL3-METTL14 in MOLM13, HEK293T, and HeLa cells.[28,30] We therefore hypothesized that ProSeMet could also be used to deposit a bioorthogonal alkyne tag (pseudomethylate) on proteins in living cells using native methyltransferases (Figure 2a). Protein extracted from T47D cells incubated with ProSeMet subjected to copper-catalyzed azide−alkyne cycloaddition (CuAAC) to attach a fluorescent picolyl azide and separated via sodium dodecyl sulfate polyacrylamide gel electrophoresis (SDS-PAGE) showed protein labeling that was detectable with as little as 5 μg of input protein (Figure 2b). Labeling efficacy scaled with increasing concentrations of ProSeMet until 100 μM concentrations were reached (Figure 2c). Since previously reported L-Met analogues have been shown to incorporate into proteins during translation,[32] we collected lysates from cells treated with L-Met, ProSeMet, or the L-Met analogue azidohomoalanine (AHA) in the presence of the protein synthesis inhibitor cycloheximide (CHX). CHX treatment abrogated AHA labeling but only slightly reduced the ProSeMet signal, indicating that the majority of ProSeMet is not incorporated into newly synthesized proteins but rather converted to ProSeAM and used by native methyltransferases (Figure 2d). To demonstrate that ProSeMet incorporation can be enzymatically driven, we examined histone H3 lysine 27 trimethylation (H3K27me3) following treatment with the EZH2 inhibitor tazemetostat in EZH2-dependent G401 cells. We selected EZH2 inhibition as EZH2 is the major methyltransferase responsible for cellular H3K27me3.[31] Under the control conditions, histone H3 is propargylated. Inhibition of EZH2 reduces both the propargylated histone H3 signal, as well as the detection of H3K27me3 (Figure 2e). Furthermore, competition with the unlabeled natural metabolite L-Met revealed a dose-dependent reduction of ProSeMet labeling with almost complete depletion of the ProSeMet signal with 10 μM L-Met (Figure 2f). Since protein methylation occurs in both the cytoplasm and nucleus, we next evaluated the cellular compartmentalization of ProSeMet-directed labeling in live cells. Cell fractionation of the cytosolic and nuclear compartments followed by SDS-PAGE fluorescent analysis revealed no fluorescent labeling of the L-Met control but robust ProSeMet labeling of proteins across molecular weights in both cytosolic and nuclear fractions (Figure 2g). We further performed immunofluorescence (IF) microscopy analysis of T47D, LNCaP, and MCF10A cells incubated with ProSeMet or L-Met. Cells treated with 100 μM ProSeMet or L-Met for 16 h were washed to remove unreacted ProSeMet, fixed, permeabilized, and ligated to a fluorophore-conjugated azide. Cells treated with ProSeMet exhibited labeling in both the cytosolic and nuclear compartments, while cells treated with L-Met remained unlabeled (Figures 2h, S1). Evaluation of condensed chromatin in mitotic cells suggests ProSeMet-directed labeling of DNA is not achieved using this approach (Figure S2). To ensure that ProSeMet would not cause cellular death during the experimental time frame, we performed Annexin V/PI staining to assess the viability of cells treated with ProSeMet over a time course. ProSeMet treatment did not increase cytotoxicity compared to dimethyl sulfoxide (DMSO) treatment at low (50 μM) or high (200 μM) concentrations (Figure S3).

Propargylated Proteins Are Identified with Site-Specific Resolution. To determine whether treatment with ProSeMet would enable the identification of propargylated proteins with site-specific resolution from live cells, the SMARCB1-deficient G401 cell line was treated with ProSeMet or L-Met over a time course of 16 to 48 h, and cellular lysates were generated, followed by protein digestion and LC-MS/MS. Proteomics analysis of digested lysates identified a total of 376 peptide spectrum matches (PSMs) in a total of 149 proteins, corresponding to 123 (82.5%) unique propargylated proteins in ProSeMet-treated samples and 27 PSMs (26 proteins, 17.5%) for L-Met (Figure 3a,b, Supplementary data 1). All instances of propargylated amino acids were observed: lysine mono-, di-, and tripropargylation, arginine mono-, and dipropargylation, and histidine monopropargylation (Figure 3c). Motif enrichment analyses suggest that lysine propargylation occurs around basic residues, arginine propargylation exhibits a slight preference for hydrophobic proximal amino acids, and histidine propargylation occurs at aliphatic and/or negatively charged sites (Figure 3d). The observed sequence motif largely corroborates previous sequence motif reports, further validating the robustness of our approach.[33] Furthermore, these sequence motif observations are of significance as they provide relevant sequence information that can be utilized in identifying protein methylation-associated writer-, reader-, and eraser-proteins.[34] Identified proteins that harbor propargylated amino acids include proteins previously known to be methylated such as HSPA8, ALDOA, and ACTG1, in addition to, and predominantly, novel protein targets and/or amino acids that have not previously been defined as methylated, including phosphoglycerate mutase 1 (PGAM1), the translation elongation factor eEF1A1, calmodulin (CALM1), the lemur tyrosine kinase LMTK3 and the 14−3−3σ adapter protein SFN (Figure 3e). Gene ontology (GO) and pathway-process enrichment analysis of propargylated proteins identified proteins involved in a variety of cellular processes including cellular response to stress, protein folding, cytoskeletal organization, protein methylation, and metabolic processes (Figures 3f, S4, Supplementary data 2). Taken together, these studies leverage the intracellular chemoenzymatic conversion of ProSeMet into ProSeAM, which is then used as a pseudomethyl donor to define known and novel amino acid propargylation events with site-specific resolution.

Enrichment of Propargylated Proteins Used to Determine the Breadth of Methylproteome. To examine the effect protein enrichment has on mapping the breadth of the methylproteome in live cells, we employed an enrichment-based approach. G401 cells were treated with ProSeMet or L-Met and cellular lysates were subjected to CuAAC to attach a biotin handle, pulled down with streptavidin beads, and analyzed via label-free LC-MS/MS (Figure S5). Using this approach, we identified 707 proteins statistically enriched at *P*-values at or below 0.05 and $\log_2$-fold change greater than 2 (Figure S6a). Of these, 486 proteins have known methylation sites and 221 have uncharacterized methylation sites (Figure S7).[35,36] Furthermore, 47 proteins were identified at *P*-values at or below 0.01 and $\log_2$-fold change greater than 5 and

https://doi.org/10.1021/jacs.4c08175
J. Am. Chem. Soc. 2025, 147, 7214−7230

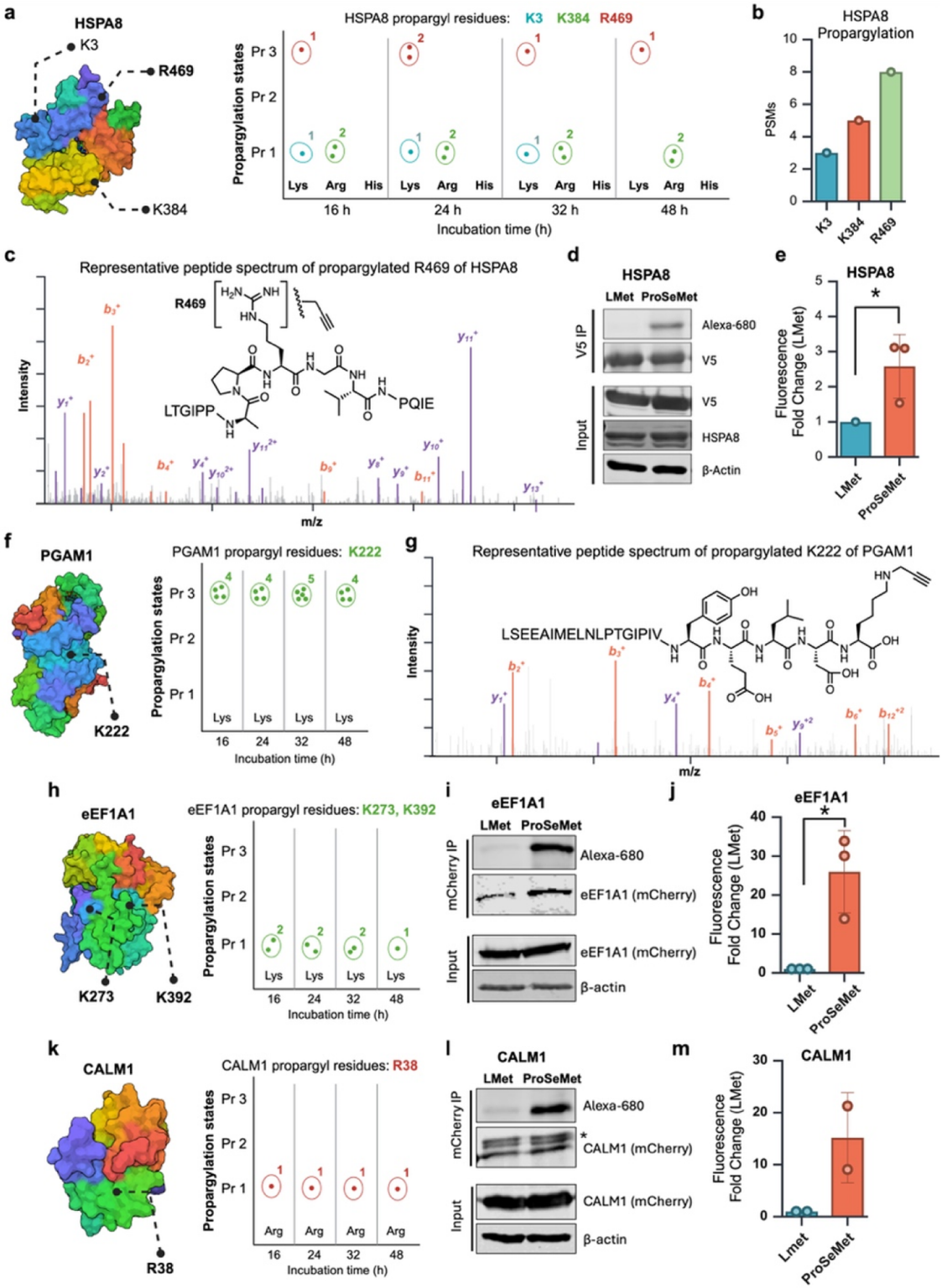

Figure 4. ProSeMet-mediated chemoproteomics identifies known and novel propargylation events. **a.** Schematic of HSPA8 propargylation states defined from G401 cells treated with ProSeMet or L-Met for 16, 24, 36, or 48 h, using LC-MS/MS. Propargylation of HSPA8 K3, K384, and R469 were observed across time points. LC-MS/MS experiments and analyses were performed with two biological replicates ($n = 2$). Propargylation sites overlaid on PDB file 2V7Z. **b**. PSM distribution of propargylated HSPA8 sites with 8 PSMs observed for HSPA8 R469me1, over 3 PSMs for HSPA8 K3me1, and HSPA8 K384me3. Analyses were performed with two biological replicates ($n = 2$). **c**. Model MS2 peptide spectrum map of HSPA8 monopropargylated R469. **d**. HSPA8-V5 immunoprecipitation with lysate from HEK293T cells treated with ProSeMet or equimolar L-Met for 24 h, followed by CuAAC to attach a fluorophore azide. **e**. Quantification of (d). ($n = 3$), *, $p \leq 0.05$. **f**. Schematic of PGAM1 propargylation states defined from G401 cells treated with ProSeMet or L-Met for 16, 24, 36, or 48 h, using LC-MS/MS. Propargylation of PGAM1 K222 was observed across time points. LC-MS/MS experiments and analyses were performed with two biological replicates ($n = 2$). Propargylation sites overlaid on PDB file 5Y2I. **g**. Model MS2 peptide spectrum map of LC-MS/MS validated PGAM1 K222 propargylation. Ectopic expression of a

https://doi.org/10.1021/jacs.4c08175
J. Am. Chem. Soc. 2025, 147, 7214−7230

Figure 4. continued

PGAM1-V5 vector in HEK293T cells, followed by treatment with L-Met or ProSeMet for 24 h, and subsequent cell lysis, V5 IP, and LC-MS/MS. **h**. Schematic of eEF1A1 propargylation states defined from G401 cells treated with ProSeMet or L-Met for 16, 24, 36, or 48 h, using LC-MS/MS. Propargylation of eEF1A1 K273me1, and K392me1 was observed across time points. LC-MS/MS experiments and analyses were performed with two biological replicates (n = 2). Propargylation sites overlaid on PDB file 1G7C. **i**. eEF1A1-mCherry immunoprecipitation with lysate from HEK293T cells treated with ProSeMet or equimolar L-Met for 24 h, followed by CuAAC to attach a fluorophore azide. **j**. Quantification of (i). (n = 3), *, $p \leq 0.05$. **k**. Schematic of CALM1 propargylation states defined from G401 cells treated with ProSeMet or L-Met for 16, 24, 36, or 48 h, using LC-MS/MS. Propargylation of CALM R38me1 was observed across time points. LC-MS/MS experiments and analyses were performed with two biological replicates (n = 2). Propargylation sites overlaid on PDB file 6YNS. **l**. CALM1-mCherry immunoprecipitation with lysate from HEK293T cells treated with ProSeMet or equimolar L-Met for 24 h, followed by CuAAC to attach a fluorophore azide. **m**. Quantification of (l). (n = 2).

includes enrichment of RNA processing proteins (SNRPD3, SNRPD1, SNRPB, SNRPE, QKI), enzymes critical to cell cycle regulation (CDK1), and several methyltransferases (CARM1, KMT2B) (Figure S6b, top 15 genes).

Network analysis of ProSeMet enriched proteins using the GO molecular signatures collection revealed a top list of GO terms involved in biological processes and molecular functions (Figure S6c). Proteins involved in methylation were highly enriched, suggesting a pulldown of proteins involved in methyl transfer as well as methyltransferase targets. This observation indicates the presence of methylation-induced modulation of the enzymatic activity of the methyltransferases. Such phenomena have been documented in previous studies where Protein Arginine Methyltransferase 1 (PRMT1)-mediated methylation of PRMT6 at R106 affects the enzymatic activity and subcellular localization of PRMT6,[37] and EZH2 methylation on K20 causing EZH2 destabilization.[38] We further observed positive enrichment of genes associated with p53-mediated signal transduction and DNA damage response (DDR) (Figure S6d). P53 is an important DNA sequence-specific transcription factor known to arrest growth by inducing apoptosis.[39] P53 activity is controlled, in part, by methylation at multiple key Lys and Arg residues: PRMT5-mediated p53 methylation at R333, R335, and R337 mediate p53 oligomerization and directly affects in DNA-induced apoptosis[40] whereas competing p53 methylation at K370/K372 by SMYD2/SETD7 can repress or enhance transcription of DDR target genes.[7,41] In addition to p53-mediated signaling, we also observed enrichment of proteins involved in RNA binding, processing, and stability, including previously identified PRMT5 targets SNRPD3, SNRPD1, and EEF1A1.[42,43] Our data supports previous studies suggesting heavy methylation of RNA-processing proteins.

Further pathway analysis using the REACTOME gene set identified gene clusters in actin dynamics, cell cycle control, WNT signaling, and transcriptional regulation (Figure S8). Within these gene clusters, we found a series of proteins involved in adhesion dynamics, including Rho GTPases RhoA, RhoG, and CDC42 and their downstream effectors, such as PAK2. Of these, only RhoA and PAK2 are known to be methylated.[35,44] We further identified key components of the WNT signaling pathway, including G3BP2, a DVL3-associated protein and positive regulator of WNT signaling that is methylated on R432, R438, R452, and R468 as well as WNT5A, which has no previously characterized methylation sites.[35,36,45] Collectively, these experiments identified dozens of known PRMT5, CARM1, EZH2, and other methyltransferase substrates in known pathways, as well as novel targets. These pre- and post-enrichment approaches highlight the prevalence of methylation in key signaling pathways and biological processes and provide a chemical proteomics scaffold to survey the methylproteome in an unbiased manner.

ProSeMet-Mediated Chemoproteomics Identifies HSPA8 Arginine Propargylation. Label-free quantification (LFQ) analysis of unenriched propargyl-containing proteins identified multiple novel and known sites of arginine, lysine, and histidine propargylation (Figure 3e, Supplementary data 1) in proteins including the constitutively expressed member of the HSP70 family of heat shock proteins HSPA8, which has essential roles in nascent protein folding as a chaperone protein.[46] Propargylation of HSPA8 was observed at three residues with monopropargylation of lysine 3 (HSPA8 K3me1), tripropargylation of lysine 384 (HSPA8 K384me3), and monopropargylation of arginine 469 (HSPA8 R469me1) (Figure 4a, Supplementary data 1, Figure S9). HSPA8 arginine propargylation (HSPA8 R469me1) was consistently observed across all time points surveyed from 16 to 48 h (Figure 4b). Among HSP70 proteins, arginine 469 (R469) is conserved and is located within the substrate binding domain, which is only accessible in the ATP-bound, open conformation.[47] Previous studies indicate that this residue undergoes monomethylation catalyzed by CARM1 and PRMT7, thus validating our observed HSPA8 R469 propargylation (Figure 4c).[47,48] PRMT7-mediated HSP70 R469me1 enhances cytoprotective mechanisms and stress response, consistent with the ability of HSP70 to bind client proteins.[47] In contrast, CARM1-directed HSP70 R469me1 has been shown to increase gene expression via recruitment of TFIIH during transcription initiation in a manner that is independent of its chaperone activity.[48]

To empirically determine whether HSPA8 is propargylated, we transiently overexpressed a V5-epitope tagged HSPA8 protein in HEK293T cells and then treated the cells with L-Met or ProSeMet for 24 h, followed by cell lysis. HSPA8 was enriched following V5 immunoprecipitation (IP), after which we used CuAAC to functionalize propargyl groups with a fluorophore-conjugated azide. The resulting proteins were then analyzed via SDS-PAGE and in-gel fluorescence. Fluorescent labeling demonstrates that HSPA8 is selectively propargylated following exposure to ProSeMet (Figure 4d,e).

ProSeMet-Mediated Chemoproteomics Identifies Novel Lysine and Arginine Propargylation. LFQ analysis of unenriched propargyl-containing proteins also identified a series of propargylation events that have not previously been defined (Figure 3e, Supplementary data 1), including the glycolytic enzyme phosphoglycerate mutase 1 (PGAM1), the translation initiation factor eEF1A1, and calcium signaling protein calmodulin (CALM1). Propargylation of PGAM1 was observed at one residue with tripropargylation of lysine 222 (PGAM1 K222me3) (Figure 4f, Supplementary data 1, Figure S9). PGAM1 K222me3 was consistently observed across all time points surveyed from 16 to 48 h (Figure 4f). We

https://doi.org/10.1021/jacs.4c08175
J. Am. Chem. Soc. 2025, 147, 7214−7230

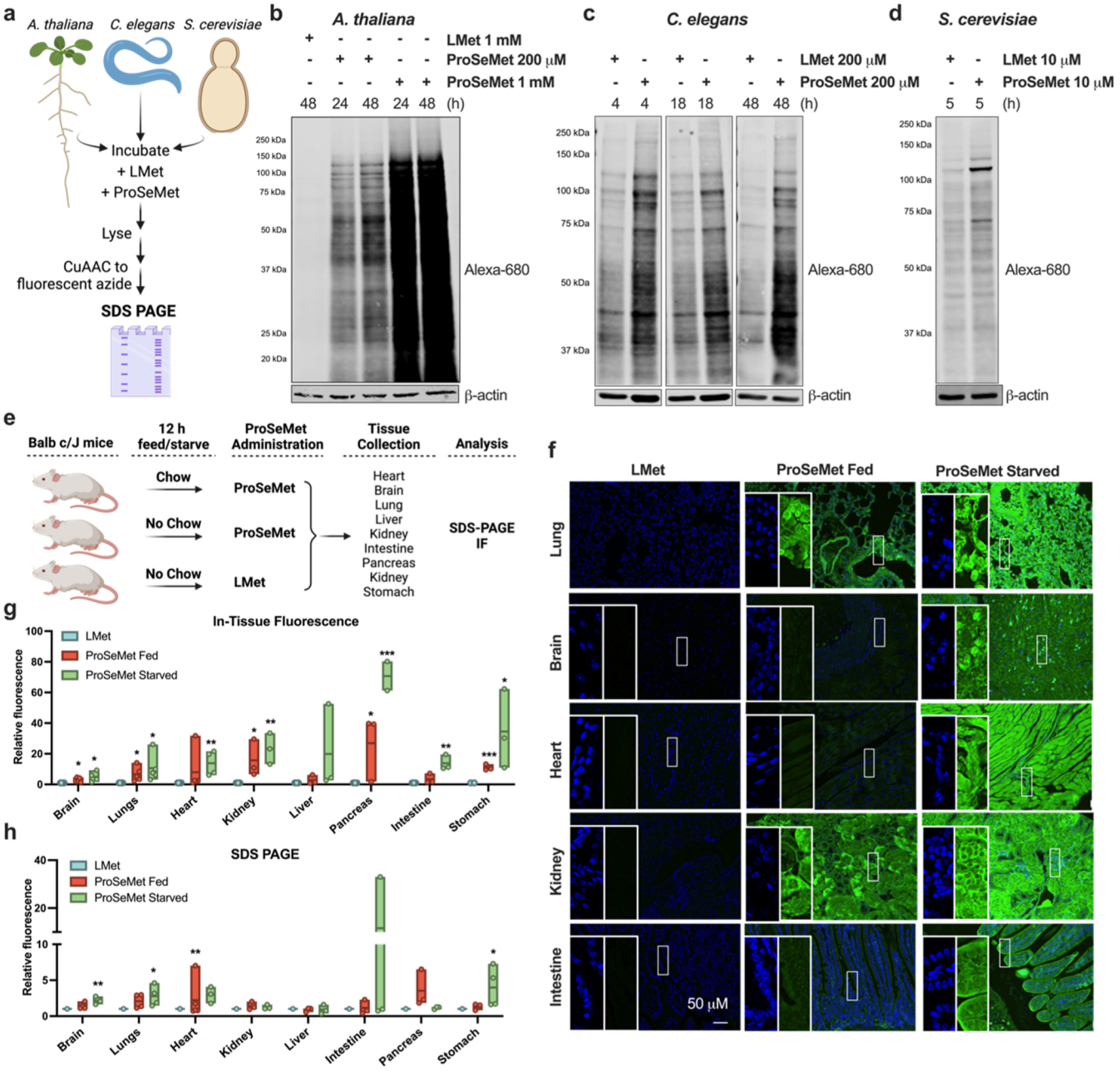

Figure 5. ProSeMet propargylates proteins *in vivo*. **a.** Schematic of the propargylation strategy in model organisms. **b**. Lysates extracted from *A. thaliana* root tips from 5-day-old seedlings treated with 200 μM or 1 mM ProSeMet or equimolar L-Met for 24 or 48 h. Lysates were subjected to CuAAC to attach a fluorescent picolyl azide (680 nm), (n = 2). **c**. Lysates extracted from *C. elegans* treated with 200 μM ProSeMet or equimolar L-Met for 4, 18, or 48 h. Lysates were subjected to CuAAC to attach a fluorescent picolyl azide (680 nm), (n = 2). **d.** Lysates extracted from *S. cerevisiae* starved for 30 min in Met, Cys-media followed by treatment with 10 μM ProSeMet or equimolar L-Met for 5 h. Lysates were subjected to CuAAC to attach a fluorescent picolyl azide (680 nm), (n = 2). **e.** Workflow for *in vivo* administration of ProSeMet or L-Met and subsequent analysis of organs for propargylation. **f**. Organs extracted from mice treated with 15 mg of ProSeMet or equimolar L-Met via IP injection while being fed or starved for 12 h were fixed in neutral buffered formalin and paraffin embedded. Tissue sections were subjected to CuAAC to attach a fluorescent picolyl azide (568 nm, pseudocolored green) and counterstained with DAPI (blue). In-tissue fluorescence analysis of the lung, brain, heart, kidneys, and intestine demonstrates successful blood−brain barrier penetrance of ProSeMet, as well as pan-organ labeling. Scalebar represents 50 μM ($n \geq 3$). **g**. Quantification of in-tissue fluorescence in the brain, heart, and lungs ($n \geq 3$). **h**. Immunoblot densitometry normalized to β-actin and relative to the L-Met control ($n \geq 3$). All tissues show increased protein labeling compared to L-Met; no significant difference was observed between mice that were fed or starved prior to ProSeMet administration. *, $p \leq 0.05$; **, $p \leq 0.01$; ***, $p \leq 0.001$.

confirmed PGAM propargylation with ectopic expression of a PGAM1-V5 vector in HEK293T cells, after which the cells were treated with L-Met or ProSeMet for 24 h, followed by cell lysis, V5 IP and LC-MS/MS (Figures 4g, S9). We also identified novel lysine and arginine propargylation events in eEF1A1 and CALM1, all of which are stable modifications that can be detected as early as 16 h: eEF1A1 K273me1 and K392me1, and CALM1 R38me1 (Figure 4h,k). eEF1A1 and CALM1 propargylation events were empirically validated by transient overexpression of a mCherry-epitope-tagged eEF1A1

https://doi.org/10.1021/jacs.4c08175
J. Am. Chem. Soc. 2025, 147, 7214−7230

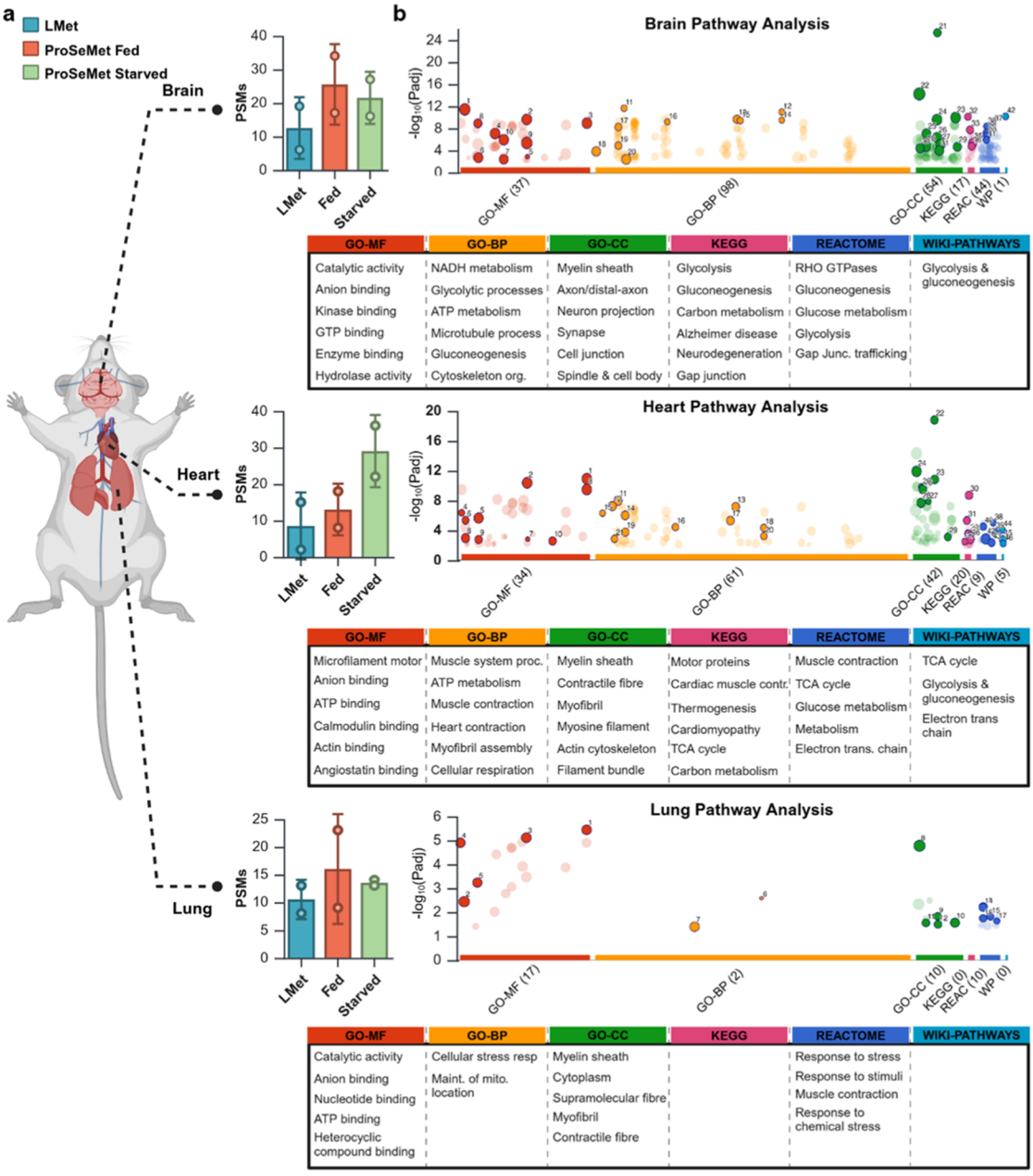

Figure 6. *In vivo* propargylation is defined with site-specific resolution. Experiments and analyses were performed with two biological replicates (n = 2). **a.** Proteomics analyses of perfused brain, heart and lung tissues from mice treated with L-Met or ProSeMet. Peptide spectral matches (PSMs) of identified propargylated amino acids in ProSeMet fed and starved samples when compared to L-Met control. All samples were filtered for contaminant hemoglobin PSMs. **b.** Gene ontology (GO) and pathway-process enrichment analysis of propargylated proteins. MS raw files were searched against the *M. musculus* Swiss-Prot database, with variable mass shifts of (+38.0157 Da for monopropargyl, +76.0314 Da for dipropargyl, and +114.0471 Da for tripropargyl) on lysine, arginine, and histidine, with a maximum propargylation state of 3 on lysine, 2 on arginine, and 1 on histidine. MF, BP, and CC are GO subontologies. GO-MF (Molecular Function, red), GO-BP (Biological Processes, yellow), GO−CC (Cellular Compartment, green), KEGG (Kyoto Encyclopedia of Genes and Genomes, pink), REACTOME (blue), and WikiPathways (cyan). Dots represent protein clusters (terms) associated with GO subontologies and circle size corresponds to term sizes. Gene list of propargylated proteins was utilized as input in metascape and gProfiler, with input and analysis species set to *M. musculus*. Pathway and process enrichment analysis was carried out with the following ontology sources: KEGG pathway, GO biological processes, reactome gene sets, canonical pathways, CORUM, WikiPathways, and PANTHER pathway. All genes in *M. musculus* genome were used as an enrichment background. Terms with $p < 0.01$, a minimum count of 3, and an enrichment factor >1.5 were utilized. p-values were calculated based on the cumulative hypergeometric distribution, and q-values were calculated using the Benjamini−Hochberg procedure.

or CALM1 protein in HEK293T cells, after which the cells were treated with L-Met or ProSeMet for 24 h, and then lysed. eEF1A1 and CALM1 were enriched from lysate with mCherry IP, after which CuAAC was used to functionalize propargyl groups with a fluorophore-conjugated azide. Fluorescent labeling demonstrates that both eEF1A1 and CALM1 are selectively propargylated following exposure to ProSeMet (Figure 4i,j, and l,m). As a control, treatment with L-Met followed by LFQ analysis of unenriched methyl-containing proteins identified methylation events for which propargylation

https://doi.org/10.1021/jacs.4c08175
J. Am. Chem. Soc. 2025, 147, 7214−7230

was also detected: eEF1A1 K273me1, eEF1A1 K392me2, and CALM1 R38me2 (Figure S9). Collectively, these data suggest that protein propargylation can serve as a surrogate for protein methylation. These data thus demonstrate the utility of our ProSeMet-driven chemoproteomics strategy to uncover existing and novel protein methylation events, thus enabling the identification of methylation-associated biological functions and disease-related biomarkers.

ProSeMet-Directed Propargylation Is Detectable *In Vivo*. The ability of ProSeMet to produce propargylated proteins *in vivo* was explored by administering ProSeMet to a series of model organisms including *A. thaliana*, *C. elegans*, *S. cerevisiae*, and *M. musculus* (Figure 5a,e). ProSeMet or L-Met was administered in growth media to *A. thaliana*, *C. elegans*, or *S. cerevisiae* and incubated for up to 48 h, after which lysates were generated and subjected to CuAAC for fluorophore conjugation. For *A. thaliana*, *C. elegans*, and *S. cerevisiae*, treatment with ProSeMet labels proteins across molecular weights (Figure 5b−d). We then administered adult male and female BALB c/J mice ProSeMet. We aimed to assess the impact of existing dietary L-Met on ProSeMet-directed labeling efficiency by dividing mice into the following cohorts: (1) dietary restriction for 12 h prior to L-Met administration; (2) no dietary restriction prior to ProSeMet administration, "fed"; or (3) dietary restriction for 12 h prior to ProSeMet administration, "starved" (Figure 5e). In all cohorts, the dietary source of L-Met was restored immediately following L-Met/ProSeMet administration. Mice were administered 15 mg of ProSeMet or the equimolar equivalent of L-Met in normal, sterile saline via intraperitoneal (IP) injection. This ProSeMet dose is equivalent to the daily dietary intake of L-Met for an adult mouse.[49] To compare the labeling efficiency between groups, tissues from a diverse array of organs were collected from mice 12 h after ProSeMet or L-Met delivery. The tissues harvested from mice in all conditions were subjected to CuAAC to attach a fluorophore-conjugated azide, then analyzed via fluorescent IHC or lysis followed by SDS-PAGE. Fluorescent labeling across organ systems demonstrates that ProSeMet can diffuse across tissues and penetrate the blood−brain barrier (BBB) (Figures 5f,h, S10). Labeling was detected in both fed mice and mice experiencing dietary restriction to reduce intracellular L-Met abundance prior to ProSeMet administration (Figures 5f,h, S10). These combined data suggest that mice starved prior to ProSeMet injection had increased levels of ProSeMet labeling in most tissues including the brain and lungs, whereas mice fed prior to ProSeMet administration had increased levels of labeling in the heart. Additional SDS-PAGE experiments suggest that ProSeMet labeling of the propargylproteome occurs as early as 3 h (data not shown). Collectively, these data demonstrate ProSeMet can be utilized in *in vivo* model organisms to propargylate proteins from both diverse model organisms across the phylogenetic tree, as well as diverse organ systems.

***In Vivo* Protein Propargylation Events Are Defined with Site-Specific Resolution.** To examine whether site-selective arginine, lysine, and histidine propargylation events can be detected *in vivo*, perfused brain, heart, and lung tissues from mice treated with L-Met or ProSeMet as described above (Figure 4e) were digested and processed for LC-MS/MS. Proteomics analyses of digested tissue-derived lysates identified an increase in propargyl sites in proteins derived from murine tissue in both the fed and starved groups (see Figure 5e for a schematic) when compared to L-Met (Figure 6a, Supplementary data 3). Mice starved prior to ProSeMet administration had increased ProSeMet labeling in the heart (Mean PSM = 29), whereas mice maintained on normal chow prior to ProSeMet administration had increased labeling in the brain (Mean PSM = 25.5) and lungs (Mean PSM = 16). These data are consistent with our bulk analyses of propargylated proteins from tissue fluorescence and SDS-PAGE (Figures 5f,h, S10), validating the reproducible nature of leveraging this ProSeMet-driven pseudomethylation strategy for methylome profiling. Network analysis of propargylated proteins using the Gene ontology (GO) and pathway-process enrichment analysis of propargylated proteins identified enrichment of propargylated proteins involved in organ-specific molecular functions, biological processes, and cellular compartmentalization (Figures 6b, S11, Supplementary data 4). Brain-associated propargylated proteins are enriched with protein clusters associated with cellular metabolism and classical neuronal function. In contrast, we observed propargylated proteins associated with structural proteins and muscle-related biological processes in the heart and metabolic and energy-related processes representative of pulmonary function, respectively. Pathway analysis of gene clusters using the KEGG, REACTOME, and WIKIPATHWAYS corroborates the observed tissue-related propargylation, with significant enrichment of neuronal- and metabolic-related pathways in the brain, muscle- and metabolic-related pathways in the heart, and signaling and muscle related pathways in the lung (Figures 6b, S11). Taken together, these observations highlight the utility of leveraging ProSeMet-driven pseudomethylation for the *in vivo* discovery of methylation events with site-specific resolution.

DISCUSSION

It is increasingly recognized that nonhistone protein methylation is an important component of cell signaling and that comprehensive characterization of the methylproteome will require the development of new experimental and analytical pipelines. Herein, we describe the application of the chemical probe ProSeMet, which can be used to propargylate proteins in the natural cellular environment. In cells, ProSeMet is enzymatically converted to ProSeAM by cellular MAT enzymes, which can subsequently be used by diverse methyltransferases in both the cytoplasm and nucleus to deposit a bioorthogonal alkyne on target proteins (Figure 1). Our approach extends previous *in situ* methodologies[24−30] to allow consideration for the biological impetus behind methylation events; this approach allows dynamic, global mapping of the methylproteome.

Using ProSeMet, we developed a reproducible platform for the analysis of protein propargylation as a surrogate for protein methylation in live cells and in diverse living organisms. For the first time, we demonstrated that ProSeMet-mediated propargylation can be detected using SDS-PAGE and confocal microscopy in cancerous (T47D, LNCaP, G401, and 293T) and untransformed (MCF10A) cell lines. Our results indicate that ProSeMet can successfully penetrate the plasma and nuclear membranes to yield labeled proteins across molecular weights (Figure 2). In addition to our *in vitro* results, we report, to our knowledge, the first application of L-Met/SAM analogues in a series of model organisms including *A. thaliana*, *C. elegans*, *S. cerevisiae*, and *M. musculus* (Figure 5), which also suggests diverse applications of ProSeMet, ranging from agriculture to mechanistic studies. To this purpose, ProSeMet was administered to Balb c/J mice via IP injection

https://doi.org/10.1021/jacs.4c08175
J. Am. Chem. Soc. 2025, 147, 7214−7230

propargylated proteins across tissues including in the heart, lungs, and brain (Figure 5). These data suggest that ProSeMet can be used to study the role of methylation in the pathophysiology of diseases affecting these and potentially other organ systems. We further hypothesize that ProSeMet can be widely leveraged in other *in vitro* and *in vivo* models.

Likewise, we developed two proteomics platforms to identify propargylated proteins, using both a native lysate as well as an eluate enriched for propargylated proteins following streptavidin precipitation. Using the SMARCB1-deficient cell line G401, we treated cells with ProSeMet or L-Met, generated cell lysate, and processed this lysate for LC-MS/MS in the absence of functionalization and enrichment. This approach identified a series of both known and novel protein propargylation events, including the heat shock chaperone protein HSPA8 and the glycolytic enzyme phosphoglycerate mutase 1 (PGAM1) (Figure 4). Some proteins within the heat shock family are ubiquitously expressed at relatively high intracellular concentrations,[50] which may explain the reproducible detection of HSPA8 R469me1 in our LC-MS/MS runs. PRMT9-mediated HSPA8 Arg (R76 and R100) methylation has been implicated in hepatocellular carcinoma,[51] and CARM1 and PRMT7 have been shown to methylate HSP70 proteins including HSPA8 on R469 in a chaperone/client independent- and dependent manner, respectively.[47,48] Our studies presented here demonstrate robust HSPA8 R469 propargylation and provide an experimental platform for future studies examining the cellular contexts of PRMT-mediated HSPA8 methylation, which when coupled with mechanistic and functional studies, are likely to provide further insight into the biological function(s) of HSPA8 R469me1. While PGAM1 lysine acetylation has been described,[52] here we provide the first evidence of PGAM1 lysine pseudomethylation at C-terminal residues including K222, K225, and K228. The reproducible detection of PGAM1 K222 through IP and LC-MS/MS further nominates PGAM1 as a novel methylation substrate. While it is unknown whether PGAM1-specific lysine methylation regulates PGAM1 function, PGAM1 overexpression has been implicated in cancer and its dysregulation may support oncogenic activity.[53] The methodologies employed here provide a platform to first define and then prioritize propargylation events for functional studies, such as examining the role of PGAM1 lysine methylation in the regulation of key steps in glycolysis. Additionally, the detection of lysine tripropargylation (e.g., PGAM1 K222me3) via the chemoenzymatic approach was unexpected; we hypothesized this propargylated species may be rare as steric hindrance of the prior two deposited propargyl groups could render the tripropargylation event sterically challenging for methyltransferases responsible for tripropargyl deposition (Figure 1c). Lastly, in addition to HSPA8 and PGAM1 propargylation, this chemoenzymatic approach defined a surrogate of all species of canonical protein methylation, including Arg, His, and Lys, as well as mono-, di-, and tripropargylation, on novel substrates including eEF1A1 and CALM1. The utility of leveraging propargylation as a proxy to detect known and novel cellular methylation events is reflected in our control label-free quantitation conditions, where samples were treated with L-Met. Using this approach, we identified methylation at some of the same sites of defined propargylation, including eEF1A1 K273me1, eEF1A1 K392me2, and CALM1 R38me2 (Figure S9). These data suggest that the tools employed herein to identify protein propargylation can serve as a surrogate for defining protein methylation events with site-specific resolution.

We also observed labeling in a variety of model organisms, demonstrating that this ProSeMet-driven chemoenzymatic approach may be amenable to use in a variety of living organisms, including and beyond those tested here. Leveraging model organisms for these studies is especially attractive given the availability of a wide variety of genetic mutant strains to examine the mechanisms of methylation as well as the benefit that model organisms such as *S. cerevisiae* encode a smaller array of methyltransferases within their genome. The latter may render these organisms as powerful tools to unmask and map both the methylproteome as well as the network of responsible methyltransferases, which is already known to have implications in disease etiologies such as cancer. The utility of complex model organisms such as murine models cannot be underscored; the observation that ProSeMet labels proteins across the blood−brain barrier as well as in all organ systems examined suggests that ProSeMet labeling in *in vivo* murine models may have applications in studying tissue-specific methylation in complex disease states such as cancer or neurological disorders. Collectively, these findings suggest broad applicability in addressing both unbiased and biased questions related to cellular methylation events *in vitro* and *in vivo*.

Using G401 cells, we then adapted our pipeline and leveraged biotin conjugation and streptavidin enrichment to define nonhistone proteins known to be methylated by PRMT1 (NONO),[54] PRMT5 (SNRPD3, SNRPD1),[43] CARM1 (SNRPB, SF3B4),[7] and EZH2 (STAT3, PCNA)[10,55] (Figure S6). We also identified the catalytic subunits (PPP2CA, PPP4C, PPP6C) of several protein phosphatases known to be methylated by the leucine carboxyl methyltransferase LCMT1.[56] In addition to these and other known methyltransferase targets, we identified 221 proteins with uncharacterized methylation sites with unknown biological function (Figure S7). Our enrichment proteomics data also indicated enrichment of the SAM synthetase enzymes MAT2A/B, which are responsible for the coupling of ATP and L-Met to produce SAM.[57] While we cannot discount the possibility that these enzymes were identified because of ProSeAM present in their binding pockets, MAT2A is purportedly methylated on a critical Arg residue in the binding pocket (R264) and this methylation event may serve as a biological switch to control cellular SAM levels.[58] Similarly, our MS data indicates the enrichment of several methyltransferases, including the Lys methyltransferases KMT2A/B, the Arg methyltransferases PRMT1, 3, 5, and CARM1, and the RNA methyltransferase NSUN2, all of which are known to be methylated.[35] To expand upon the approaches taken here, future chemoproteomics analyses of ProSeMet targets could focus on the elucidation of the molecular mechanisms by which methylation of methyltransferases controls their function. While the studies herein identify enzymes involved in methylation, a limitation is the ability to comprehensively determine whether all cellular methyltransferases can utilize ProSeAM as a propargyl donor. Prior studies suggest ProSeAM serves as a propargyl donor for at least some m6A-depositing RNA methyltransferases,[28,29] and work by other groups employ a targeted *in situ* approach in which ProSeAM functions as a propargyl donor for select protein methyltransferases.[25,26,59] Here we build upon these data and identify lysine, arginine, and histidine propargylation events in living

https://doi.org/10.1021/jacs.4c08175
J. Am. Chem. Soc. 2025, 147, 7214−7230

cells and organisms, which suggest that diverse methyltransferase families can utilize ProSeAM as a propargyl donor. Orthogonal approaches such as pharmacological inhibition of the EZH2 methyltransferase suggest that EZH2 also uses ProSeAM as a propargyl donor (Figure 2). While this approach is not comprehensive, we hypothesize that many, if not most, protein methyltransferases can utilize ProSeAM as a propargyl donor, and this may be due in part to the architecture of the methyl-binding pocket of protein methyltransferases. Future studies could leverage this methodology in targeted approaches that employ purified methyltransferases with substrate peptides in *in situ* reactions to define the breadth and depth of protein methyltransferases that utilize ProSeAM as a propargyl donor.

The ProSeMet pipelines described herein allow profiling of methyltransferase targets *in vitro* and *in vivo* while allowing a comprehensive survey of canonical and noncanonical propargylated residues. Other proteomic approaches have been employed to survey the methylproteome, including pan-methyl, pan-methyl lys, and pan-methyl arg antibody-based enrichment,[16] alone and in combination with the use of isotopic labeling.[15] Early studies paired culturing cells with deuterated methionine to produce heavy-methylated substrates, which could be enriched via pan-methyl antibody affinity purification and LC-MS/MS. This heavy-SILAC approach identified 59 methylation events in a total of 33 proteins.[15] Subsequent pan monomethyl-lys, dimethyl-lys, and trimethyl-lys antibody enrichment followed with LC-MS/MS identified a total of 552 methylation events on 413 methylated proteins, most of which are implicated in chromatin biology.[16] This powerful antibody affinity purification approach benefits from unique antibodies for each methylation state, with limitations including antibody cross-reactivity and with SILAC, possible background associated with cotranslational incorporation of deuterated methionine. Recent studies surveying affinity reagents using peptide microarray suggest that pan-methyl lys antibodies exhibit sequence bias, and that employing multiple different pan-methyl lys antibodies enhances the robustness of results; this approach identified more than 5089 methylated lysine residues on 2751 proteins.[60] Our approach has several advantages over previous methodologies: ProSeMet readily enters live cells and whole organisms; ProSeMet-mediated propargylation considers the biological impetus for a methylation event; ProSeMet and the corresponding SAM analogue ProSeAM can be used by native methyltransferases in cell lines and *in vivo*; and the CuAAC reaction allows for identification of all propargylated amino acid states in a single tube, with or without enrichment, via LC-MS/MS. This platform provides a new avenue to dissect the methylation-controlled crosstalk and signal transduction responsible for cellular function.

METHODS

Synthesis of ProSeMet. Propargyl-selenium L-methionine (ProSeMet) was synthesized following a previously described protocol[61] with modified purification method. L-selenohomocystine (200 mg, 0.55 mmol) was dissolved in dry ethanol (25 mL), $NaBH_4$ (126 mg, 3.30 mmol) was added under nitrogen, and the reaction mixture was stirred at room temperature (RT) for 15 min. $NaHCO_3$ (152 mg, 3.3 mmol) was added to the reaction mixture in one portion, followed by propargyl bromide (250 μL, 3.3 mmol), and the resultant reaction mixture was stirred at RT for 12 h. The solvent was removed under reduced pressure, and the crude compound was dissolved in distilled water (6 mL) and 1% trifluoroacetic acid (TFA, 60 μL). The resulting solution was directly loaded to neutral alumina, and then 50% EtOAc and hexane (50 mL) were used to wash the nonpolar impurities, followed by 50% methanol and dichloromethane (DCM, 50 mL) to remove polar impurities. ProSeMet was eluted by NH_4OH solution (50 mL) from a neutral alumina column, which was concentrated and lyophilized to afford the pure product (92 mg, 76%).

ESI-MS. Expected mass for $C_7H_{11}NO_2SeK^+$: 259.24 $[M + K]^+$; found: 259.815. (Figure S12).

^{1}H NMR. ^{1}H NMR (600 MHz, D_2O) δ 3.84−3.81 (m, 1H), 3.30 (s, 2H), 2.84 (t, J = 8.0 Hz, 2H), 2.64 (s, 1H), 2.30−2.20 (m, 2H) (Figure S13).

^{13}C NMR. (151 MHz, D_2O) δ: 175.29, 54.90, 54.64, 31.67, 19.30, 19.09, 6.31. (Figure S14).

Cell Culture. Cells were purchased from ATCC and maintained at 37 °C and 5% CO_2. HEK293T, T47D, LNCaP, and G401 cells were cultured in either Dulbecco's modified Eagle's medium (DMEM) or RPMI supplemented with 10% (V/V) fetal bovine serum (FBS) and 1% (V/V) penicillin/streptomycin (pen/strep) (100 μg/mL). MCF10A cells were cultured in DMEM/F-12 supplemented with 3% (V/V) FBS, cholera toxin (100 ng/mL), EGF (20 ng/mL), hydrocortisone (0.5 mg/mL), insulin (10 μg/mL), and 1% (V/V) pen/strep. For L-Met depletion experiments, cells were cultured in cysteine- and methionine-free DMEM (Gibco 21013024) supplemented with pen/strep, L-Cystine 2HCl (63 mg/mL), and dialyzed serum (Gibco A3382001). Cycloheximide (CHX) was purchased from Sigma (01810).

Cell and Organism Lysis and Immunoblotting. *H. sapiens* whole cell lysate was generated by lysing cells on ice in radioimmunoprecipitation assay (RIPA) buffer (50 mM Tris-HCl [pH 8], 150 mM NaCl, 1% NP-40, 0.5% sodium deoxycholate, and 0.1% SDS) supplemented with protease and phosphatase inhibitors. Histones were acid extracted from G401 cells as described previously.[62] Briefly, cells were lysed on ice in a Triton extraction buffer (TEB; PBS, 0.5% Triton X-100). Cell lyses were centrifuged at 6,500g at 4 °C and proteins including histones were acid extracted from the pellet via 1:1 TEB:0.8 N HCl. Proteins including histones were centrifuged at 4 °C and the proteins precipitated from the supernatant following the addition of an equal volume of 50% TCA, then centrifuged at 12,000g at 4 °C. Precipitated proteins were washed once in ice-cold 0.3 N HCl in acetone and twice with ice-cold acetone before lyophilization. Dried proteins were resuspended in 20 mM Tris-HCl (pH 8.0) and 0.4 N NaOH, supplemented with protease inhibitors. *A. thaliana* whole cell lysate was generated by grinding 1 g of root tissue to a powder in liquid N_2 in a mortar and pestle and then lysing with 1 mL of RIPA buffer with further grinding. The suspension was then filtered through a 70 μM cell strainer and centrifuged at 1200g for 5 min at 4 °C, and the supernatant obtained after centrifugation was used as a protein lysate. *C. elegans* whole organism lysate was generated by lysing nematodes in RIPA buffer, including 25 cycles of douching. Lysates were centrifuged at 16,000g for 10 min at 4 °C, and soluble lysate was collected. *S. cerevisiae* whole cell lysate was generated by lysing cells in an RIPA buffer. Lysates were centrifuged 6500g, 10 min at 4 °C, and soluble lysate was collected. Protein lysate concentration was determined by the Bradford Assay (BioRad). Proteins were prepared in 1X LDA sample buffer (Invitrogen) containing 10% β-mercaptoethanol and then were separated using 12 or 16% SDS-PAGE. When applicable, proteins were Alexa-680-fluorophore labeled via CuAAC (ClickChemistryTools #1511). Proteins were then transferred to nitrocellulose membranes and visualized directly via fluorophore or visualized after blocking in TBST + 5% Milk, primary antibody incubation (Odyssey and Li-Cor), and secondary antibody incubation. Primary antibodies used were as follows: β-actin (1:1000, Millipore-Sigma MAB1501), V5 (1:1000, CST80076), HSPA8 (1:1000, CST8444S), H3K27me3 (1:1000, CST 9733), H3 (1:1000, Abcam 1791), mCherry (1:1000, Abcam 213511) and HDAC1 (1:1000, Upstate 05-614). Secondary antibodies used include the fluorophore-conjugated goat antirabbit 680 IgG (Licor 925-68071) and goat antimouse 800 IgG (LiCor 926-32210).

Copper-Catalyzed Azide−Alkyne Cycloaddition (CuAAC) Reaction. CuAAC on whole cell lysate, fixed cells, or tissue sections was

https://doi.org/10.1021/jacs.4c08175
J. Am. Chem. Soc. 2025, 147, 7214−7230

performed using 1 mM $CuSO_4$, 1.5 mM THPTA, 3 mM sodium ascorbate (NaAsc), and indicated concentration of azide (Table S1). All azides and alkynes were purchased from ClickChemistryTools. For whole cell lysate, CuAAC reagents were added directly to the lysate, incubated for 30 or 60 min at RT, and then prepared for downstream analysis. For confocal microscopy, cells were fixed in 3.7% paraformaldehyde (PFA) and permeabilized with 0.5% Triton X-100. CuAAC reagents were added directly to cells and then incubated, rocking, for 45 min. For IHC, tissue sections were permeabilized as described below, and CuAAC reagents supplemented with 5% DMSO and 0.2% Triton X-100 were added directly to the tissue section for 1 h prior to proceeding with the confocal microscopy pipeline described below.

Biotin–Streptavidin Pulldown. G401 cells were incubated in L-Met free media for 30 min, treated with 100 μM ProSeMet or L-Met for 16 h, and then lysed with RIPA buffer. Protein lysate (1 mg/IP) was diluted to 1 mL final volume in PBS, then subjected to CuAAC for 1 h at RT to attach an azide-conjugated biotin moiety (ClickChemistryTools #1167-25). After CuAAC, the protein was precipitated in acetone. Briefly, 4 volumes of ice-cold acetone were added to the post-CuAAC lysate, followed by incubation at −20 °C for 1 h. Precipitated proteins were centrifuged at 9000*g* for 10 min and resuspended in PBS with 5% SDS. After resuspension, the SDS solution was diluted to 0.5% in PBS, and then magnetic streptavidin beads (Pierce) were added directly to the resuspended protein. Protein and beads were incubated for 2 h at RT, rocking, and then beads were washed 3X with ice-cold RIPA buffer and 3X with ice-cold PBS. Beads with attached proteins were stored at −80 °C until LC-MS/MS analysis.

Immunoprecipitation. HEK293T cells were transiently transfected with the following plasmids: HSPA8_pLX307 (Addgene Plasmid #98343), pLX304 Flag-mCherry-eEF1A1 (Addgene Plasmid #198383), or pCAG mCherry-mCalmodulin1 (Addgene Plasmid #127393). 48 h post-transfection, cells were washed twice in 1X PBS, incubated in Cysteine free medium (Invitrogen) for 30 min, and then treated with 200 μM ProSeMet or L-Met for 24 h. At 72 h post-transfection, cells were lysed with RIPA buffer. Protein lysate (4.5 mg) was diluted in IP Buffer (20 mM Tris pH 7.5, 150 mM NaCl, 5 mM $MgCl_2$, 1% NP-40) for immunoprecipitation (IP) with 0.84 μg V5 antibody (CST80076) or 1 μg mCherry antibody (Abcam 213511) and 40 μL washed Protein A or Protein G beads (Invitrogen). Post IP, beads were washed in IP Buffer, followed by PBS, and resuspended in 1X LDS before boiling for 5 min at 95 °C. Denatured proteins were loaded into a centrifugal 30 kDa filter (Millipore), and diluted with 400 μL of dH_2O. Filters were spun at 10,000 rpm for 10 min, 200 μL of H_2O was added, and spun at 10,000 rpm for 10 min. Remaining volume containing proteins was subjected to CuAAC for 30 min at RT to attach an azide-conjugated fluorophore. After CuAAC, proteins were loaded into a centrifugal 30 kDa filter, diluted with 300 μL of H_2O, and spun for 10 min at 10,000 rpm. 200 μL of additional H_2O was added, and the filter was spun at 10,000 rpm for 25 min. The remaining solution containing proteins was separated by using SDS-PAGE, and immunoblots were performed as described above.

Annexin V/PI Staining. T47D cells were incubated with 5 or 20 μM of ProSeMet for 24 h, detached with accutase (Biolegend), and stained using Annexin V/PI following manufacturer's protocol (Biolegend). Cells were analyzed via a flow cytometer (BDFACSymphony A3) within 1 h.

Confocal Microscopy. Live cells were plated, and after 16 h, cells were washed to remove excess L-Met and incubated in methionine-free supplemented DMEM (Gibco) for 30 min to remove endogenous methionine. Subsequently, 100 or 200 μM concentrations of ProSeMet was added to the cells. After 16 h, cells were fixed with 4% PFA and permeabilized using 0.5% Triton X-100. The CuAAC reaction was then performed directly on the fixed and permeabilized cells as described to attach a 488 or 568 nm picolyl azide-conjugated fluorophore (ClickChemistryTools #1275-1, #1291-5) and nuclei were counterstained using Hoechst. Cells were imaged on a Leica SP8 confocal microscope, and images were processed and analyzed using ImageJ and Python.

Mass Spectrometry. *Mass Spectrometry for Unenriched Samples. Sample Preparation.* ProSeMet and L-Met modified lysates were digested using an EasyPrep Mini MS Sample Prep Kit (Thermo Scientific). 100 μg of proteins were treated with 50 μL of reduction and 50 μL of alkylation buffer and then incubated at 95 °C for 10 min in the dark. Reduced and alkylated protein samples were cooled to RT and digested with a digestion cocktail of 50 μL of (trypsin and Lys-C) or 50 μL of (Glu-C) for 24 h. The resulting peptides were desalted with an EasyPep Mini MS peptide cleanup column (Thermo Scientific) and dried under vacuum.

LC-MS/MS for Unenriched Samples. Digested samples were resuspended in Buffer A (0.1% FA in water) and the peptide amount was determined by Pierce Quantitative Peptide Assays & Standards (ThermoFisher Scientific) according to the manufacture's instructions. Samples were injected into a nanoElute UPLC autosampler (Bruker Daltonics) coupled to a timsTOF Pro2 mass spectrometer (Bruker Daltonics). The peptides were loaded on a 25 cm Aurora ultimate CSI C18 column (IonOpticks) and chromatographic separation was achieved using a linear gradient starting with a flow rate of 250 nL/min from 2% Buffer B (0.1% FA in MeCN) and increasing to 13% in 42 min, followed by an increase to 23% B in 65 min, 30% B in 70 min, then the flow rate was increased to 300 nL/min and 80% B in 85 min, this was kept for 5 min. The mass spectrometer operated in positive polarity for data collection using a data-dependent acquisition (ddaPASEF) mode. The cycle time was 1.17 s and consisted of one full scan followed by 10 PASEF/MSMS scans. Precursors with intensity of over 2500 (arbitrary units) were picked for fragmentation and precursors over the target value of 20,000 were dynamically excluded for 1 min. Precursors below 700 Da were isolated with a 2 Th window and ones above with 3 Th. All spectra were acquired within an m/z range of 100 to 1700 and fragmentation energy was set to 20 eV at 0.6 1/K0 and 59 eV at 1.60 1/K0.

Database Search (MSFragger). MS raw files were searched with FragPipe GUI version 20 with MSFragger (version 3.8) as the search algorithm. Protein identification was performed with the human Swiss-Prot database (20′456 entries) with acetylation (N-terminus), and oxidation on methionine was set variable modification. To account for the mass shift introduced by the propargyl handle, a variable mass shift of 38.0157 Da on Lysine, Arginine, and Histidine with a maximal occurrence of 3 propargyl, respectively, was set. Carbamidomethylation of cysteine residues was considered to be a fixed modification. Trypsin or Glu-C was set as the enzyme with up to two missed cleavages. The peptide length was set to 7–50, and the peptide mass range of 500–5000 Da. For MS2-based experiments, the precursor tolerance was set to 20 ppm, and fragment tolerance was set to 20 ppm. Peptide spectrum matches were adjusted to a 1% false discovery rate using Percolator as part of the Philosopher toolkit (v5). For label-free quantification, match-between-runs were enabled. All downstream analysis was performed in R (version 2023.03.0). Individual samples were normalized to the mean of all of the quantified peptides.

Data Analysis. For the unenriched pipeline, following a database search with MSFragger, contaminant proteins were filtered, and PSMs with zero intensities and Match type of "unmatched" were removed. Blood-related hemoglobin PSMs were filtered from mouse peptide data. For Gene Ontology (GO) analysis of G401 cells, gene list of propargylated proteins were utilized as input in metascape, with input and analysis species set to *H. sapiens*. For GO analysis of the murine model, a gene list of propargylated proteins was utilized as input in metascape[63] and gProfiler, with input and analysis species set to *M. musculus*. Pathway and process enrichment analysis was carried out with the following ontology sources: KEGG Pathway, GO Biological Processes, Reactome Gene Sets, Canonical Pathways, CORUM, WikiPathways, and PANTHER Pathway. All genes in the human and mouse genomes were used as the enrichment background. Terms with a p-value <0.01, a minimum count of 3, and an enrichment factor >1.5 were utilized. p-values were calculated based on the cumulative hypergeometric distribution, and q-values are calculated using the Benjamini–Hochberg procedure. To identify the sequence motif of

https://doi.org/10.1021/jacs.4c08175
J. Am. Chem. Soc. 2025, 147, 7214–7230

ProSeMet modified sites, "probability logo generator for biological sequence motif plogo v1.2.0 was utilized. Sequences containing 5 residues from the left and 4 residues from the right of modified lysine and arginine sites were utilized, with lysine or arginine as the fixed positions with a p-value <0.05. For sequence motif analysis of histidine, sequences containing 4 residues from the left and 4 residues from the right of modified histidine sites were utilized.

Mass Spectrometry for Enriched Samples. Sample Preparation. On-bead digestion was performed as previously described.[64] To the beads was added digestion buffer (50 mM NH_4HCO_3) and the mixture was then treated with 1 mM dithiothreitol (DTT) at RT for 30 min, followed by 5 mM iodoacetimide (IAA) at RT for 30 min in the dark. Proteins were digested with 2 μg of lysyl endopeptidase (Wako) at RT overnight and were further digested overnight with 2 μg trypsin (Promega) at RT. The resulting peptides were desalted using an HLB column (Waters) and were dried under vacuum.

LC-MS/MS for Enriched Samples. The data acquisition by LC-MS/MS was adapted from a published procedure.[65] Derived peptides were resuspended in the loading buffer (0.1% trifluoroacetic acid, TFA) and were separated on a Water's Charged Surface Hybrid (CSH) column (150 μm internal diameter (ID) × 15 cm; particle size: 1.7 μm). The samples were run on an EVOSEP liquid chromatography system using the 15 samples per day preset gradient (88 min) and were monitored on a Q-Exactive Plus Hybrid Quadrupole-Orbitrap Mass Spectrometer (ThermoFisher Scientific). The mass spectrometer cycle was programmed to collect one full MS scan, followed by 20 data-dependent MS/MS scans. The MS scans (400−1600 m/z range, 3×10^6 AGC target, 100 ms maximum ion time) were collected at a resolution of 70,000 at m/z 200 in profile mode. The HCD MS/MS spectra (1.6 m/z isolation width, 28% collision energy, 1×10^5 AGC target, 100 ms maximum ion time) were acquired at a resolution of 17,500 at m/z 200. Dynamic exclusion was set to exclude previously sequenced precursor ions for 30 s. Precursor ions with +1, +7, +8, or higher charge states were excluded from sequencing.

MaxQuant. Relative intensity values were calculated from raw data using MaxQuant. Label-free quantification analysis was adapted from a published procedure.[65] Spectra were searched using the search engine Andromeda, integrated into MaxQuant, against Human Uniprot/Swiss-Prot database (20,379 target sequences). Methionine oxidation (+15.9949 Da), asparagine and glutamine deamidation (+0.9840 Da), and protein N-terminal acetylation (+42.0106 Da) were variable modifications (up to 5 allowed per peptide); cysteine was assigned as a fixed carbamidomethyl modification (+57.0215 Da). Only fully tryptic peptides were considered with up to 2 missed cleavages in the database search. A precursor mass tolerance of ±20 ppm was applied prior to mass accuracy calibration and ±4.5 ppm after internal MaxQuant calibration. Other search settings included a maximum peptide mass of 6000 Da, a minimum peptide length of 6 residues, 0.05 Da tolerance for orbitrap, and 0.6 Da tolerance for ion trap MS/MS scans. The false discovery rate (FDR) for peptide spectral matches, proteins, and site decoy fraction were all set to 1%. Quantification settings were as follows: requantify with a second peak finding attempt after protein identification has completed; match MS1 peaks between runs; a 0.7 min retention time match window was used after an alignment function was found with a 20 min RT search space. Quantitation of proteins was performed using summed peptide intensities given by MaxQuant. The quantitation method considered only razor plus unique peptides for protein-level quantitation.

Data Analysis. For the enrichment pipeline, following MaxQuant, all data was log2-transformed before further analysis. Contaminant proteins were filtered, and missing values were imputed using a normal distribution in Perseus. Differential protein expression was performed on normalized intensity values using the DEqMS R package (https://www.bioconductor.org/packages/release/bioc/html/DEqMS.html).[66] Samples with a high level of variance calculated using PCA were removed (Figure S7). GSEA was performed on enriched proteins (LFC > 1) using the fgsea R package (https://bioconductor.org/packages/release/bioc/html/fgsea.html). Data sets with $\log_2$-transformed fold changes were analyzed using C5 (GO) and C2 (REACTOME) gene set collections in the Molecular Signatures Database (MSigDB v 7.5.1). Identification of proteins with known or unknown methylation sites was performed by cross-referencing the PhosphoSitePlus and ActiveDriver DB databases.[67]

***In Vivo* Studies.** *C. elegans.* N2 wild-type (Bristol isolate) *C. elegans* were cultured at 20 °C on 60 mm nematode growth medium (NGM) agar plates with OP50 bacteria grown in Luria Broth (LB). Mixed stage worms were washed into liquid OP50 grown in LB and maintained by shaking at moderate speed at 20 °C for 10 days, refreshing the OP50 bacteria at 5 days. The resulting population was washed by allowing the worms to sink via gravity and replacing the M9 buffer (22 mM KH_2PO_4, 42 mM Na_2HPO_4, 86 mM NaCl, and 1 mM $MgSO_4$) approximately 5 times or until the liquid ran clear. Worms were then starved by shaking in M9 buffer without bacteria at 20 °C for 4 h, pelleted, and then added to fresh OP50 with either L-Met or ProSeMet at a final concentration of 200 μM. Worms were collected at 4, 18, and 48 h after starvation was ended by pelleting and washing with M9 buffer approximately 5 times or until liquid ran clear. A final volume of 500uL M9 containing whole worms was flash-frozen with liquid nitrogen and stored at −80 °C until lysis.

A. thaliana. Col-0 ecotype seeds were sterilized and sown on 1/2 Murashige and Skoog (MS) medium supplemented with 1% (w/v) sucrose. The seedlings were grown on plates in the vertical orientation in a controlled growth chamber under 16 h light/8 h dark cycles, at a temperature of 20 °C, and light intensity of 200 μmol/m^2/s for 5 days after germination. After 5 days, seedlings were treated with 10 mL of MS media containing either 200 μM or 1 mM ProSeMet or L-Met by pouring the liquid onto the plates and swirling. Plates were then returned to the growth chamber and kept in a horizontal orientation for 24 or 48 h. Whole roots from the treated seedlings were then harvested and immediately frozen in liquid N_2 for protein extraction.

S. cerevisiae. S288C cells (MATa; ura3-52; leu2Δ1; HIS3; trp1Δ63) were grown in complete YEPD medium with overnight shaking at 30 °C. Cells were then diluted to OD = 0.1 in Met/Cys medium and starved for 30 min, and L-Met or ProSeMet was then added at 10 μM concentrations. When the cells reached OD = 1 (about 6.5 h), pellets were flash-frozen. Pellets were resuspended in RIPA buffer (50 mM Tris-HCl pH 8.0, 150 mM NaCl, 1% NP-40, 0.5% Na deoxycholate, and 0.1% SDS) supplemented with protease inhibitors. Cells were lysed by beating with 0.3 mg of acid washed glass beads for 1 min with 2 min rest on ice, 4 times. Lysates were clarified via centrifugation at 14,000 rpm at 4 °C for 10 m.

M. musculus. Male and female BALB c/J mice (Jackson laboratories) were maintained on a standard chow diet. 12 h prior to L-Met or ProSeMet delivery, mice were either starved or maintained on the standard chow diet, after which they were administered 15 mg of ProSeMet or equimolar L-Met, resuspended in sterile 0.9N saline, via intraperitoneal (IP) injection. At the time of ProSeMet or L-Met administration, standard chow was returned. Mice were monitored hourly postadministration and euthanized after 12 h. All tissue collected was isolated and prepared within 1 h following euthanasia. All mouse experiments were conducted in accordance with protocols approved by the Institutional Animal Care and Use Committee (IACUC) of the Emory University School of Medicine (EUCM).

In-Tissue Fluorescence. Organs extracted from mice treated with ProSeMet or L-Met were immediately placed in a 4% formaldehyde solution and left at RT for 24 h. Subsequently, organs were paraffin embedded and sectioned. Tissue slides were rehydrated by washing 3 times with xylenes (mixed isomers), twice with 100% EtOH, once with 95% EtOH, once with 80% EtOH, once with 70% EtOH, and once with PBS. All washes were for 5 m. After the final wash, tissue sections were permeabilized by using 0.5% TX-100 in PBS for 1 h. After permeabilization, CuAAC was performed directly on slides using 1 mM CuSO4, 1.5 mM THPTA, 3 mM NaAsc, 25 μM picolyl azide conjugated to a 568 nm fluorophore (ClickChemistryTools #1291-5), 5% DMSO, and 0.2% TX-100, for 1 h at RT. After the reaction completed, slides were washed for 30 min in PBS supplemented with 5% DMSO and 0.2% TX-100, then for 30 min in PBS. Slides were then stained with DAPI (300 nM) for 5 min at RT. Prior to

https://doi.org/10.1021/jacs.4c08175
J. Am. Chem. Soc. 2025, 147, 7214−7230

mounting, slides were dehydrated by washing once with 70% EtOH, once with 80% EtOH, twice with 100% EtOH, and twice with xylenes (mixed isomers). All washes were for 5 m. After dehydration, slides were mounted and imaged using a confocal microscope (Leica SP8).

■ ASSOCIATED CONTENT

Data Availability Statement

Correspondence and requests for materials should be addressed to Dr. Jennifer M. Spangle, Ph.D., Jennifer.spangle@emory.edu.

Supporting Information

The Supporting Information is available free of charge at https://pubs.acs.org/doi/10.1021/jacs.4c08175.

Additional experimental details and images, and 1H NMR spectra for all compounds (PDF)

■ AUTHOR INFORMATION

Corresponding Author

Jennifer M. Spangle − *Department of Radiation Oncology, Winship Cancer Institute of Emory University School of Medicine, Atlanta, Georgia 30322, United States;* orcid.org/0000-0002-0181-3244; Email: Jennifer.spangle@emory.edu

Authors

Jonathan Farhi − *Department of Radiation Oncology, Winship Cancer Institute of Emory University School of Medicine, Atlanta, Georgia 30322, United States; Cancer Biology Program, Emory University, Atlanta, Georgia 30322, United States; Department of Chemistry, Emory University, Atlanta, Georgia 30322, United States*

Benjamin Emenike − *Department of Chemistry, Emory University, Atlanta, Georgia 30322, United States*

Richard S. Lee − *Department of Radiation Oncology, Winship Cancer Institute of Emory University School of Medicine, Atlanta, Georgia 30322, United States*

Kirti Sad − *Department of Radiation Oncology, Winship Cancer Institute of Emory University School of Medicine, Atlanta, Georgia 30322, United States*

Dorelle V. Fawwal − *Biochemistry, Cell, and Developmental Biology Program, Emory University, Atlanta, Georgia 30322, United States*

Christian M. Beusch − *Department of Pathology and Laboratory Medicine, Emory University School of Medicine, Atlanta, Georgia 30322, United States*

Robert B. Jones − *Department of Radiation Oncology, Winship Cancer Institute of Emory University School of Medicine, Atlanta, Georgia 30322, United States*

Ashish K. Verma − *Department of Chemistry, Emory University, Atlanta, Georgia 30322, United States*

Celina Y. Jones − *Department of Biology, Emory College of Arts and Sciences, Atlanta, Georgia 30322, United States*

Maryam Foroozani − *Department of Biology, Emory College of Arts and Sciences, Atlanta, Georgia 30322, United States*

Monica Reeves − *Department of Cell Biology, Emory University, Atlanta, Georgia 30322, United States;* orcid.org/0000-0002-6222-4865

Kiran K. Parwani − *Department of Radiation Oncology, Winship Cancer Institute of Emory University School of Medicine, Atlanta, Georgia 30322, United States; Cancer Biology Program, Emory University, Atlanta, Georgia 30322, United States*

Pritha Bagchi − *Emory Integrated Proteomics Core, Emory University, Atlanta, Georgia 30322, United States*

Roger B. Deal − *Department of Biology, Emory College of Arts and Sciences, Atlanta, Georgia 30322, United States*

David J. Katz − *Department of Cell Biology, Emory University, Atlanta, Georgia 30322, United States*

Anita H. Corbett − *Department of Biology, Emory College of Arts and Sciences, Atlanta, Georgia 30322, United States*

David E. Gordon − *Department of Pathology and Laboratory Medicine, Emory University School of Medicine, Atlanta, Georgia 30322, United States*

Monika Raj − *Department of Chemistry, Emory University, Atlanta, Georgia 30322, United States;* orcid.org/0000-0001-9636-2222

Complete contact information is available at: https://pubs.acs.org/10.1021/jacs.4c08175

Author Contributions

◆The authors J.F. and B.E. contributed equally.

Notes

The authors declare no competing financial interest.

■ ACKNOWLEDGMENTS

The authors thank Dr. David Lynn, Dr. Andrew Hong, and the Spangle, Raj, and Hong laboratories for helpful project discussions. This study was supported by funds from Winship Cancer Institute of Emory University and the NIH (1R35GM150587), to J.M.S. M.R. acknowledges funding from NIH (1R35GM133719-01). The *S. cerevisiae* work performed by C.Y.J. was funded by the NIH (K12 GM000680, to C.Y.J.). The *C. elegans* work performed by M.R. (T32GM008490-21) was funded by a grant to D.J.K. (NSF IOS1354998). This study was supported in part by the Emory University Cancer Tissue Pathology Core and Integrated Proteomics Core facility (RRID:SCR_023530), both of which are shared resources of Winship Cancer Institute of Emory University and the NIH/NCI (P30CA138292). The indicated figures were created using BioRender. [Figure 3 (License PF26RS7R7U), Figure 4 (License ZG26T7IHR3), Figure 5a (License WJ26RQFQ1T), Figure 5e (License NP26RQN94I), and Figure 6 (License PK26RS9KSL).

■ REFERENCES

(1) Murn, J.; Shi, Y. The winding path of protein methylation research: milestones and new frontiers. *Nat. Rev. Mol. Cell Biol.* **2017**, *18* (8), 517−527.

(2) Michalak, E. M.; Burr, M. L.; Bannister, A. J.; Dawson, M. A. The roles of DNA, RNA and histone methylation in ageing and cancer. *Nat. Rev. Mol. Cell Biol.* **2019**, *20* (10), 573−589.

(3) Fontecave, M.; Atta, M.; Mulliez, E. S-adenosylmethionine: nothing goes to waste. *Trends Biochem. Sci.* **2004**, *29* (5), 243−249.

(4) Bedford, M. T. Arginine methylation at a glance. *J. Cell Sci.* **2007**, *120* (24), 4243−4246.

(5) Bannister, A. J.; Kouzarides, T. Regulation of chromatin by histone modifications. *Cell Res.* **2011**, *21* (3), 381−395.

(6) Wu, Z.; Connolly, J.; Biggar, K. K. Beyond histones - the expanding roles of protein lysine methylation. *FEBS J.* **2017**, *284* (17), 2732−2744.

(7) Biggar, K. K.; Li, S. S. Non-histone protein methylation as a regulator of cellular signalling and function. *Nat. Rev. Mol. Cell Biol.* **2015**, *16* (1), 5−17.

(8) Guo, J.; Dai, X.; Laurent, B.; Zheng, N.; Gan, W.; Zhang, J.; Guo, A.; Yuan, M.; Liu, P.; Asara, J. M.; et al. AKT methylation by SETDB1

promotes AKT kinase activity and oncogenic functions. *Nat. Cell Biol.* **2019**, *21* (2), 226−237.
(9) Chan, L. H.; Zhou, L.; Ng, K. Y.; Wong, T. L.; Lee, T. K.; Sharma, R.; Loong, J. H.; Ching, Y. P.; Yuan, Y. F.; Xie, D.; et al. PRMT6 Regulates RAS/RAF Binding and MEK/ERK-Mediated Cancer Stemness Activities in Hepatocellular Carcinoma through CRAF Methylation. *Cell Rep.* **2018**, *25* (3), 690−701 e698.
(10) Kim, E.; Kim, M.; Woo, D. H.; Shin, Y.; Shin, J.; Chang, N.; Oh, Y. T.; Kim, H.; Rheey, J.; Nakano, I.; et al. Phosphorylation of EZH2 activates STAT3 signaling via STAT3 methylation and promotes tumorigenicity of glioblastoma stem-like cells. *Cancer Cell* **2013**, *23* (6), 839−852.
(11) He, A.; Shen, X.; Ma, Q.; Cao, J.; von Gise, A.; Zhou, P.; Wang, G.; Marquez, V. E.; Orkin, S. H.; Pu, W. T. PRC2 directly methylates GATA4 and represses its transcriptional activity. *Genes Dev.* **2012**, *26* (1), 37−42.
(12) Park, S. H.; Fong, K. W.; Kim, J.; Wang, F.; Lu, X.; Lee, Y.; Brea, L. T.; Wadosky, K.; Guo, C.; Abdulkadir, S. A.; et al. Posttranslational regulation of FOXA1 by Polycomb and BUB3/USP7 deubiquitin complex in prostate cancer. *Sci. Adv.* **2021**, *7* (15 DOI: 10.1126/sciadv.abe2261.
(13) Hoy, S. M. Tazemetostat: First Approval. *Drugs* **2020**, *80* (5), 513−521.
(14) Siu, L. L.; R, D.; Vinay, S. P.; Romano, P. M.; Menis, J.; Opdam, F. L.; Heinhuis, K. M.; Egger, J. L.; Gorman, S. A.; Parasrampuria, R.; Wang, K.; Kremer, B. E.; Gounder, M. M. METEOR-1: A phase I study of GSK3326595, a first-in-class protein arginine methyltransferase 5 (PRMT5) inhibitor, in advanced solid tumours. *Ann. Oncol.* **2019**, *30*.
(15) Ong, S. E.; Mittler, G.; Mann, M. Identifying and quantifying in vivo methylation sites by heavy methyl SILAC. *Nat. Methods* **2004**, *1* (2), 119−126.
(16) Cao, X. J.; Arnaudo, A. M.; Garcia, B. A. Large-scale global identification of protein lysine methylation in vivo. *Epigenetics* **2013**, *8* (5), 477−485.
(17) Guo, A.; Gu, H.; Zhou, J.; Mulhern, D.; Wang, Y.; Lee, K. A.; Yang, V.; Aguiar, M.; Kornhauser, J.; Jia, X.; et al. Immunoaffinity enrichment and mass spectrometry analysis of protein methylation. *Mol. Cell Proteomics* **2014**, *13* (1), 372−387.
(18) Levy, D.; Liu, C. L.; Yang, Z.; Newman, A. M.; Alizadeh, A. A.; Utz, P. J.; Gozani, O. A proteomic approach for the identification of novel lysine methyltransferase substrates. *Epigenetics Chromatin* **2011**, *4*, 19.
(19) Bremang, M.; Cuomo, A.; Agresta, A. M.; Stugiewicz, M.; Spadotto, V.; Bonaldi, T. Mass spectrometry-based identification and characterisation of lysine and arginine methylation in the human proteome. *Mol. Biosyst* **2013**, *9* (9), 2231−2247.
(20) Hart-Smith, G.; Yagoub, D.; Tay, A. P.; Pickford, R.; Wilkins, M. R. Large Scale Mass Spectrometry-based Identifications of Enzyme-mediated Protein Methylation Are Subject to High False Discovery Rates. *Mol. Cell Proteomics* **2016**, *15* (3), 989−1006.
(21) Nwajiobi, O.; Mahesh, S.; Streety, X.; Raj, M. Selective Triazenation Reaction (STaR) of Secondary Amines for Tagging Monomethyl Lysine Post-Translational Modifications. *Angew. Chem., Int. Ed.* **2021**, *60* (13), 7344−7352.
(22) Chalker, J. M.; Bernardes, G. J.; Davis, B. G. A "tag-and-modify" approach to site-selective protein modification. *Acc. Chem. Res.* **2011**, *44* (9), 730−741.
(23) Islam, K. The Bump-and-Hole Tactic: Expanding the Scope of Chemical Genetics. *Cell Chem. Biol.* **2018**, *25* (10), 1171−1184.
(24) Wang, R.; Islam, K.; Liu, Y.; Zheng, W.; Tang, H.; Lailler, N.; Blum, G.; Deng, H.; Luo, M. Profiling genome-wide chromatin methylation with engineered posttranslation apparatus within living cells. *J. Am. Chem. Soc.* **2013**, *135* (3), 1048−1056.
(25) Peters, W.; Willnow, S.; Duisken, M.; Kleine, H.; Macherey, T.; Duncan, K. E.; Litchfield, D. W.; Luscher, B.; Weinhold, E. Enzymatic site-specific functionalization of protein methyltransferase substrates with alkynes for click labeling. *Angew. Chem., Int. Ed.* **2010**, *49* (30), 5170−5173.
(26) Sohtome, Y.; Shimazu, T.; Shinkai, Y.; Sodeoka, M. Propargylic Se-adenosyl-l-selenomethionine: A Chemical Tool for Methylome Analysis. *Acc. Chem. Res.* **2021**, *54* (20), 3818−3827.
(27) Davydova, E.; Shimazu, T.; Schuhmacher, M. K.; Jakobsson, M. E.; Willemen, H.; Liu, T.; Moen, A.; Ho, A. Y. Y.; Malecki, J.; Schroer, L.; et al. The methyltransferase METTL9 mediates pervasive 1-methylhistidine modification in mammalian proteomes. *Nat. Commun.* **2021**, *12* (1), 891.
(28) Hartstock, K.; Nilges, B. S.; Ovcharenko, A.; Cornelissen, N. V.; Pullen, N.; Lawrence-Dorner, A. M.; Leidel, S. A.; Rentmeister, A. Enzymatic or In Vivo Installation of Propargyl Groups in Combination with Click Chemistry for the Enrichment and Detection of Methyltransferase Target Sites in RNA. *Angew. Chem., Int. Ed.* **2018**, *57* (21), 6342−6346.
(29) Muttach, F.; Rentmeister, A. A Biocatalytic Cascade for Versatile One-Pot Modification of mRNA Starting from Methionine Analogues. *Angew. Chem., Int. Ed.* **2016**, *55* (5), 1917−1920.
(30) Mikutis, S.; Gu, M.; Sendinc, E.; Hazemi, M. E.; Kiely-Collins, H.; Aspris, D.; Vassiliou, G. S.; Shi, Y.; Tzelepis, K.; Bernardes, G. J. L. meCLICK-Seq, a Substrate-Hijacking and RNA Degradation Strategy for the Study of RNA Methylation. *ACS Cent Sci.* **2020**, *6* (12), 2196−2208.
(31) Knutson, S. K.; Warholic, N. M.; Wigle, T. J.; Klaus, C. R.; Allain, C. J.; Raimondi, A.; Porter Scott, M.; Chesworth, R.; Moyer, M. P.; Copeland, R. A.; et al. Durable tumor regression in genetically altered malignant rhabdoid tumors by inhibition of methyltransferase EZH2. *Proc. Natl. Acad. Sci. U.S.A.* **2013**, *110* (19), 7922−7927.
(32) Dieterich, D. C.; Link, A. J.; Graumann, J.; Tirrell, D. A.; Schuman, E. M. Selective identification of newly synthesized proteins in mammalian cells using bioorthogonal noncanonical amino acid tagging (BONCAT). *Proc. Natl. Acad. Sci. U.S.A.* **2006**, *103* (25), 9482−9487.
(33) Chen, Z.; Liu, X.; Li, F.; Li, C.; Marquez-Lago, T.; Leier, A.; Akutsu, T.; Webb, G. I.; Xu, D.; Smith, A. I.; et al. Large-scale comparative assessment of computational predictors for lysine post-translational modification sites. *Brief Bioinform* **2019**, *20* (6), 2267−2290.
(34) Hyun, K.; Jeon, J.; Park, K.; Kim, J. Writing, erasing and reading histone lysine methylations. *Exp Mol. Med.* **2017**, *49* (4), No. e324.
(35) Hornbeck, P. V.; Zhang, B.; Murray, B.; Kornhauser, J. M.; Latham, V.; Skrzypek, E. PhosphoSitePlus, 2014: mutations, PTMs and recalibrations. *Nucleic Acids Res.* **2015**, *43* (Database issue), D512−520.
(36) Krassowski, M.; Paczkowska, M.; Cullion, K.; Huang, T.; Dzneladze, I.; Ouellette, B. F. F.; Yamada, J. T.; Fradet-Turcotte, A.; Reimand, J. ActiveDriverDB: human disease mutations and genome variation in post-translational modification sites of proteins. *Nucleic Acids Res.* **2018**, *46* (D1), D901−D910.
(37) Cao, M. T.; Feng, Y.; Zheng, Y. G. Protein arginine methyltransferase 6 is a novel substrate of protein arginine methyltransferase 1. *World J. Biol. Chem.* **2023**, *14* (5), 84−98.
(38) Guo, P.; Lim, R. C.; Rajawasam, K.; Trinh, T.; Sun, H.; Zhang, H. A methylation-phosphorylation switch controls EZH2 stability and hematopoiesis. *eLife* **2024**, *13*. DOI: DOI: 10.7554/eLife.86168.
(39) Menendez, D.; Inga, A.; Resnick, M. A. The expanding universe of p53 targets. *Nat. Rev. Cancer* **2009**, *9* (10), 724−737.
(40) Jansson, M.; Durant, S. T.; Cho, E. C.; Sheahan, S.; Edelmann, M.; Kessler, B.; La Thangue, N. B. Arginine methylation regulates the p53 response. *Nat. Cell Biol.* **2008**, *10* (12), 1431−1439.
(41) Chuikov, S.; Kurash, J. K.; Wilson, J. R.; Xiao, B.; Justin, N.; Ivanov, G. S.; McKinney, K.; Tempst, P.; Prives, C.; Gamblin, S. J.; et al. Regulation of p53 activity through lysine methylation. *Nature* **2004**, *432* (7015), 353−360.
(42) Fong, J. Y.; Pignata, L.; Goy, P. A.; Kawabata, K. C.; Lee, S. C.; Koh, C. M.; Musiani, D.; Massignani, E.; Kotini, A. G.; Penson, A.; et al. Therapeutic Targeting of RNA Splicing Catalysis through Inhibition of Protein Arginine Methylation. *Cancer Cell* **2019**, *36* (2), 194−209 e199.

(43) Meister, G.; Eggert, C.; Buhler, D.; Brahms, H.; Kambach, C.; Fischer, U. Methylation of Sm proteins by a complex containing PRMT5 and the putative U snRNP assembly factor pICln. *Curr. Biol.* **2001**, *11* (24), 1990−1994.
(44) Hodge, R. G.; Ridley, A. J. Regulating Rho GTPases and their regulators. *Nat. Rev. Mol. Cell Biol.* **2016**, *17* (8), 496−510.
(45) Bikkavilli, R. K.; Malbon, C. C. Wnt3a-stimulated LRP6 phosphorylation is dependent upon arginine methylation of G3BP2. *J. Cell Sci.* **2012**, *125* (Pt 10), 2446−2456.
(46) Stricher, F.; Macri, C.; Ruff, M.; Muller, S. HSPA8/HSC70 chaperone protein: structure, function, and chemical targeting. *Autophagy* **2013**, *9* (12), 1937−1954.
(47) Szewczyk, M. M.; Ishikawa, Y.; Organ, S.; Sakai, N.; Li, F.; Halabelian, L.; Ackloo, S.; Couzens, A. L.; Eram, M.; Dilworth, D.; et al. Pharmacological inhibition of PRMT7 links arginine monomethylation to the cellular stress response. *Nat. Commun.* **2020**, *11* (1), 2396.
(48) Gao, W. W.; Xiao, R. Q.; Peng, B. L.; Xu, H. T.; Shen, H. F.; Huang, M. F.; Shi, T. T.; Yi, J.; Zhang, W. J.; Wu, X. N.; et al. Arginine methylation of HSP70 regulates retinoid acid-mediated RARbeta2 gene activation. *Proc. Natl. Acad. Sci. U.S.A.* **2015**, *112* (26), E3327−3336.
(49) Brown-Borg, H. M. Reduced growth hormone signaling and methionine restriction: interventions that improve metabolic health and extend life span. *Ann. N.Y. Acad. Sci.* **2016**, *1363*, 40−49.
(50) Hu, C.; Yang, J.; Qi, Z.; Wu, H.; Wang, B.; Zou, F.; Mei, H.; Liu, J.; Wang, W.; Liu, Q. Heat shock proteins: Biological functions, pathological roles, and therapeutic opportunities. *MedComm 2020* **2022**, *3* (3), No. e161.
(51) Deng, W.; Ai, J.; Zhang, W.; Zhou, Z.; Li, M.; Yan, L.; Zhang, L.; Huang, Z.; Wu, Z.; Ai, J.; et al. Arginine methylation of HSPA8 by PRMT9 inhibits ferroptosis to accelerate hepatitis B virus-associated hepatocellular carcinoma progression. *J. Transl. Med.* **2023**, *21* (1), 625.
(52) Hallows, W. C.; Yu, W.; Denu, J. M. Regulation of glycolytic enzyme phosphoglycerate mutase-1 by Sirt1 protein-mediated deacetylation. *J. Biol. Chem.* **2012**, *287* (6), 3850−3858.
(53) Sun, Q.; Li, S.; Wang, Y.; Peng, H.; Zhang, X.; Zheng, Y.; Li, C.; Li, L.; Chen, R.; Chen, X.; et al. Phosphoglyceric acid mutase-1 contributes to oncogenic mTOR-mediated tumor growth and confers non-small cell lung cancer patients with poor prognosis. *Cell Death Differ.* **2018**, *25* (6), 1160−1173.
(54) Yin, X. K.; Wang, Y. L.; Wang, F.; Feng, W. X.; Bai, S. M.; Zhao, W. W.; Feng, L. L.; Wei, M. B.; Qin, C. L.; Wang, F.; et al. PRMT1 enhances oncogenic arginine methylation of NONO in colorectal cancer. *Oncogene* **2021**, *40* (7), 1375−1389.
(55) A, P.; Xu, X.; Wang, C.; Yang, J.; Wang, S.; Dai, J.; Ye, L. EZH2 promotes DNA replication by stabilizing interaction of POLdelta and PCNA via methylation-mediated PCNA trimerization. *Epigenetics Chromatin* **2018**, *11* (1), 44.
(56) Hwang, J.; Lee, J. A.; Pallas, D. C. Leucine Carboxyl Methyltransferase 1 (LCMT-1) Methylates Protein Phosphatase 4 (PP4) and Protein Phosphatase 6 (PP6) and Differentially Regulates the Stable Formation of Different PP4 Holoenzymes. *J. Biol. Chem.* **2016**, *291* (40), 21008−21019.
(57) Singh, S.; Zhang, J.; Huber, T. D.; Sunkara, M.; Hurley, K.; Goff, R. D.; Wang, G.; Zhang, W.; Liu, C.; Rohr, J.; et al. Facile chemoenzymatic strategies for the synthesis and utilization of S-adenosyl-(L)-methionine analogues. *Angew. Chem., Int. Ed.* **2014**, *53* (15), 3965−3969.
(58) Massignani, E.; Giambruno, R.; Maniaci, M.; Nicosia, L.; Yadav, A.; Cuomo, A.; Raimondi, F.; Bonaldi, T. ProMetheusDB: An In-Depth Analysis of the High-Quality Human Methyl-proteome. *Mol. Cell Proteomics* **2022**, *21* (7), No. 100243.
(59) Willnow, S.; Martin, M.; Luscher, B.; Weinhold, E. A selenium-based click AdoMet analogue for versatile substrate labeling with wild-type protein methyltransferases. *Chembiochem* **2012**, *13* (8), 1167−1173.
(60) Berryhill, C. A.; Hanquier, J. N.; Doud, E. H.; Cordeiro-Spinetti, E.; Dickson, B. M.; Rothbart, S. B.; Mosley, A. L.; Cornett, E. M. Global lysine methylome profiling using systematically characterized affinity reagents. *Sci. Rep.* **2023**, *13* (1), 377.
(61) Hartstock, K.; Nilges, B. S.; Ovcharenko, A.; Cornelissen, N. V.; Pllen, N.; Lawrence-Drner, A.-M.; Leidel, S. A.; Rentmeister, A. Enzymatic or in vivo installation of propargyl groups in combination with click chemistry for the enrichment and detection of methyltransferase target sites in RNA. *Angew. Chem., Int. Ed.* **2018**, *57* (21), 6342−6346.
(62) Jones, R. B.; Farhi, J.; Adams, M.; Parwani, K. K.; Cooper, G. W.; Zecevic, M.; Lee, R. S.; Hong, A. L.; Spangle, J. M. Targeting MLL Methyltransferases Enhances the Antitumor Effects of PI3K Inhibition in Hormone Receptor-positive Breast Cancer. *Cancer Res. Commun.* **2022**, *2* (12), 1569−1578.
(63) Zhou, Y.; Zhou, B.; Pache, L.; Chang, M.; Khodabakhshi, A. H.; Tanaseichuk, O.; Benner, C.; Chanda, S. K. Metascape provides a biologist-oriented resource for the analysis of systems-level datasets. *Nat. Commun.* **2019**, *10* (1), 1523.
(64) Soucek, S.; Zeng, Y.; Bellur, D. L.; Bergkessel, M.; Morris, K. J.; Deng, Q.; Duong, D.; Seyfried, N. T.; Guthrie, C.; Staley, J. P. Evolutionarily conserved polyadenosine RNA binding protein Nab2 cooperates with splicing machinery to regulate the fate of pre-mRNA. *Mol. Cell. Biol.* **2016**, *36* (21), 2697−2714.
(65) Seyfried, N. T.; Dammer, E. B.; Swarup, V.; Nandakumar, D.; Duong, D. M.; Yin, L.; Deng, Q.; Nguyen, T.; Hales, C. M.; Wingo, T. A multi-network approach identifies protein-specific co-expression in asymptomatic and symptomatic Alzheimer's disease. *Cell Systems* **2017**, *4* (1), 60−72. e64.
(66) Zhu, Y.; Orre, L. M.; Tran, Y. Z.; Mermelekas, G.; Johansson, H. J.; Malyutina, A.; Anders, S.; Lehtiö, J. DEqMS: a method for accurate variance estimation in differential protein expression analysis. *Molecular Cellular Proteomics* **2020**, *19* (6), 1047−1057.
(67) Hornbeck, P. V.; Zhang, B.; Murray, B.; Kornhauser, J. M.; Latham, V.; Skrzypek, E. PhosphoSitePlus, 2014: mutations, PTMs and recalibrations. *Nucleic Acids Res.* **2015**, *43* (D1), D512−D520.

https://doi.org/10.1021/jacs.4c08175
J. Am. Chem. Soc. 2025, 147, 7214−7230